Tailoring the excited-state energy landscape in supramolecular nanostructures

Kreger, Klaus; Schmidt, Hans-Werner; Hildner, Richard

Published in:
Electronic structure

DOI:
10.1088/2516-1075/abf485

Publication date:
2021

TOPICAL REVIEW • OPEN ACCESS

Tailoring the excited-state energy landscape in supramolecular nanostructures

To cite this article: Klaus Kreger *et al* 2021 *Electron. Struct.* **3** 023001

Electronic Structure

OPEN ACCESS

RECEIVED
8 December 2020

REVISED
20 February 2021

ACCEPTED FOR PUBLICATION
1 April 2021

PUBLISHED
16 June 2021

TOPICAL REVIEW

Tailoring the excited-state energy landscape in supramolecular nanostructures

Klaus Kreger[1], **Hans-Werner Schmidt**[1,*] and **Richard Hildner**[2,*]

[1] Macromolecular Chemistry and Bavarian Polymer Institute, University of Bayreuth, Universitätsstraße 30, 95447 Bayreuth, Germany
[2] Zernike Institute for Advanced Materials, University of Groningen, Nijenborgh 4, 9747 AG Groningen, The Netherlands
[*] Authors to whom any correspondence should be addressed.

E-mail: hans-werner.schmidt@uni-bayreuth.de and r.m.hildner@rug.nl

Keywords: excited-state energy landscape, H-aggregate, J-aggregate, supramolecular nanostructure, optical spectroscopy, exciton energy transport, superstructures

Abstract

Nature's photosynthetic machinery uses precisely arranged pigment-protein complexes, often representing superstructures, for efficient light-harvesting and transport of excitation energy (excitons) during the initial steps of photosynthesis. This function is achieved by defined electronic Coulomb interactions between the conjugated molecules resulting in tailored excited-state energy landscapes. While such complex natural structures are synthetically difficult to achieve, supramolecular chemistry is now on its advent to realize defined artificial supramolecular nanostructures with tailored functionalities via controlled self-assembly processes of small molecules. In this review, we focus on recent work reporting photophysical studies on self-assembled and hierarchical nanostructures as well as complex superstructures. We discuss how the resulting excited-state energy landscapes influence energy transport. Progress in the field of supramolecular chemistry allows for the realization of distinct kinds of H- or J-aggregates with well-defined morphologies on the mesoscale. Advances in the field of optical spectroscopy and microscopy have permitted to resolve the incoherent/coherent dynamics of exciton transport in such systems down to the level of single nanostructures. Although outstanding diffusion lengths of up to several μm were found in selected nanostructures, a full understanding of the underlying principles is still missing. In particular, the unavoidable structural and electronic disorder in these systems influences the excited-state energy landscapes and thus the transport characteristics, which can be exploited to refine the molecular design criteria of supramolecular nanostructures and complex superstructures. Despite the rapid progress in the field of functional supramolecular nanostructures, we believe that revealing the full potential of such systems is far from complete. In particular, criteria for tailored and optimized (hierarchical) supramolecular nanostructures in view of applications are not yet established. Finally, we outline current challenges and future perspectives for optical and optoelectronic applications of supramolecular nanostructures.

1. Introduction

Nature uses intriguing concepts for the efficient conversion of sunlight into a useful form of chemical energy. The versatility of nature's photosynthetic machinery remains unsurpassed so far, and photosynthetic organisms, such as plants, bacteria and algae, survive in partially extreme habitats. A striking example are green sulphur bacteria in the deep sea near black smokers, thriving on photosynthesis from only a few hundreds of photons per second, 14 orders of magnitude less than the Sun's irradiance on the Earth's surface [1]. Survival under such conditions requires efficient absorption of light energy as well as efficient transport of excitation energy towards transducing units, the chemical reaction centres. Those processes occur in the photosynthetic apparatus that often comprises sophisticated pigment-protein complexes [2–4]. Within such complexes, conjugated organic molecules, such as different (bacterio)chlorophylls, tetrapyrroles (bilins) and carotenoids, are

precisely arranged into a dense network, often within a protein scaffold, and thus these complexes represent pigment-protein superstructures.

To make efficient use of the incident sunlight, nature exploits several tricks that are related to the excited-state energy landscape created in such pigment-protein structures: first, since the excited-state energy of the molecules depends on their chemical structure, only those molecules are incorporated into pigment-protein complexes that are able to absorb in the spectral range of the light incident at the habitat of the organism. Often not more than two chemically different molecules are found in pigment-protein complexes, e.g., a carotenoid (spheroidene, rhodopin glucoside, okenone) and bacteriochlorophyll a in the photosynthetic apparatus of purple bacteria [2, 3]. Second, non-covalent interactions of the conjugated organic molecules with the protein matrix, in particular with polar protein residues, induce energy level shifts and modify the molecules' transition energy by several tens to hundreds of cm^{-1}. Such energy level shifts allow to fine-tune the molecular absorption to the spectrum of the incident light. Finally, the dense and precise packing of molecules within pigment-protein structures gives rise to the formation of delocalised electronic excitations (molecular excitons), mediated by intermolecular electronic Coulomb interactions between the molecules' transition dipole moments. The excited-state energy of excitons is shifted with respect to that of the non-interacting molecules. This additional energy-level shift allows nature for a final level of fine-tuning the absorption spectrum of the pigment-protein structures, and/or to extend the spectral range for light absorption beyond what can be achieved with only one or two species of non-interacting molecules. The change in the excited-state energies by carefully tuned pigment-protein and pigment–pigment interactions also creates an energy gradient in the excited-state energy landscape to direct excitation energy in a highly efficient manner towards the reaction centres [3, 5]. This directed transport of excitation energy within pigment-protein complexes can involve several hundreds of molecules and can occur across distances in the range of 100 nm, in extraordinary cases up to 2 μm [2], with a quantum efficiency close to unity [6].

An intriguing aspect in nature's design of light-harvesting systems is the exploitation of quantum effects, because those emerge in 'warm, messy and anything but controlled' environments [7]. In this context, the most prominent effect is the formation of delocalised excitons, mediated by electronic Coulomb interactions between molecules in densely packed and well-defined arrangements. Excitation energy is then coherently shared between many molecules, which is often referred to as quantum coherent (wave-like) energy transport. This delocalisation makes energy available over a large part of a light-harvesting complex, which probably plays an important role in the robustness and overall quantum efficiency of photosynthesis [6, 4,8–10].

An important lesson to be learnt from nature is that optimised function, i.e., light-energy conversion and energy transport is closely related to a highly defined arrangement of the building blocks, in particular of the pigment molecules [3,5,6, 4,9–12]. This function thus arises from the cooperative properties of many interacting molecules within a supramolecular nano- or superstructure, rather than from those of the individual building blocks. However, many key factors in this direction are still not fully understood, e.g. the precise role of the excited-state energy landscape and of quantum coherence for efficient energy transport, as well as the influence of electronic and structural disorder, of the local environment, of the dimensionality of the structures, and the mutual interplay of these factors [6, 4,8–10, 13–15]. From the material science point of view, the synthesis of sophisticated large molecules (i.e., sequence-controlled polymers as found in nature), which are capable of forming precisely defined nanostructures with specific functions has not been realized yet [16]. Consequently, research in the field of supramolecular chemistry is dedicated to the investigation of assemblies of small molecules. However, materials and physical concepts, in particular to study and make use of effects, such as quantum coherence in artificial systems, are still rare.

Box: terms and definitions used in this review.

Molecular exciton: collective excited state with singlet character in a densely packed assembly of organic conjugated molecules, created by electronic Coulomb interactions between their transition dipole moments (see section 2.1).
Transition/site energy: energy difference between the lowest electronically excited and electronic ground state of a molecule within a nanostructure, if the intermolecular Coulomb interaction were absent (see section 2.1).
Molecule/building block/monomer: entire molecule, including the photoactive part and the peripheral groups, which is able to form supramolecular nanostructures/polymers under suitable processing conditions.
Chromophore: the conjugated, photoactive part of a molecule without peripheral (solubilising) groups.

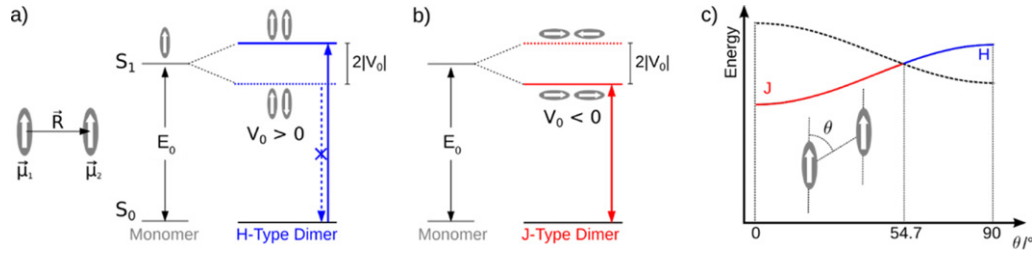

Figure 1. Kasha model of two identical interacting organic molecules. Each molecule (monomer) is depicted by its TDM μ (TDM, white arrows in grey ellipses), and the close proximity gives rise to an electronic Coulomb interaction V_0 between the TDMs depending on the mutual arrangement of the molecules. (a) H-type dimer with a face-to-face arrangement and a positive Coulomb interaction, $V_0 > 0$. The optically allowed exciton state is the upper state, and since the emission always stems from the lowest-energy excited state an ideal H-type dimer is entirely non-emissive. (b) J-type dimer with a head-to-tail arrangement and a negative interaction, $V_0 < 0$. The optically allowed exciton state is the lower energy one, which is thus responsible for absorption and emission. In (a) and (b) energy level shifts of the dimer due to Coulomb interaction (or van-der-Waals binding) energies in the ground and excited states [23, 24] have been neglected for simplicity. Those shifts are often called gas-to-crystal shifts [19], and the corresponding interactions are referred to as non-resonant (London) dispersion interactions. (c) Dependence of the energies of the optically allowed (solid line) and forbidden exciton states (dashed line) as function of the slip angle θ between the monomers' TDMs.

Supramolecular nanostructure/supramolecular polymer: well-defined nano- to mesoscale assembly of building blocks (monomers) held together by non-covalent, directional and reversible interactions (see section 2.2).
Type of aggregates/nanostructures: H- or J- (type) aggregates formed by a specific building block (see section 2.1).
Kind of aggregates/nanostructures: specific type (H- or J-type) of a nanostructure based on the same building block, but with a (slightly) different structural arrangement and thus photophysical properties (see section 2.2.2).
Morphology of nanostructures: shape of a supramolecular nanostructure on the nano- and mesoscale comprising distinct types and kinds of aggregates (see sections 2.2.2 and 3).
Hierarchical nanostructures and complex superstructures: hierarchical structures refer to objects, which feature a higher level of aggregation based on supramolecular nanostructures (see section 3.1). Complex hierarchical structures composed of *different* (supramolecular) nanostructures will here be referred to as complex superstructures (see section 3.3).

In this article we review the current state-of-the-art in designing and tuning the excited-state energy landscape in artificial functional supramolecular nanostructures. We specifically focus on reviewing recent work that combines photophysical (spectroscopic/microscopic) studies on self-assembled and hierarchically structured systems as well as complex superstructures with energy transport measurements on excited states with singlet character. Reference to triplet states is only made where appropriate. In section 2.1, we will briefly discuss the theory of the photophysics of supramolecular assemblies introducing the main concepts. Section 2.2 provides selected examples of self-assembled systems, based on molecular design principles, and discusses their spectroscopic properties. In section 3 we show how hierarchical self-assembly of supramolecular nanostructures increases the level of complexity, and allows to manipulate the excited-state energy landscape. We also demonstrate how long-range exciton transport is established in supramolecular nanostructures. Section 4 outlines potential applications and future perspectives of complex supramolecular nanostructures.

2. From single molecules to supramolecular nanostructures: molecular excitons and their optical properties

2.1. Photophysics of supramolecular assemblies: H- and J-aggregates

In this section we will briefly discuss how the excited-state energy landscape and the photophysics of supramolecular nanostructures are determined by the precise mutual arrangement of the building blocks, by electronic interactions, and by coupling to intramolecular vibrational modes. We focus on a qualitative description of the main effects, detailed mathematical derivations can be found elsewhere [3, 17–22].

Starting with the simplest approach, we describe the basic phenomena using a dimer-model with two identical interacting organic molecules (figure 1). Each molecule is approximated as a two-level system comprising the electronic ground S_0 and first excited state S_1. The energy difference between those electronic states is E_0

and the associated transition dipole moment (TDM) is non-zero, $\mu \neq 0$, which makes the $S_0 \leftrightarrow S_1$ transition optically allowed. Here we will refer to this simple picture as 'Kasha-picture', introduced in the 1960ies [20, 21], although basic concepts of molecular excitons were also developed by Davydov [22]. A close proximity of both molecules gives rise to a significant electronic Coulomb interaction V_0 between the molecules' TDMs, which is usually described in the point-dipole approximation with its characteristic R^{-3} distance dependence (figure 1(a)). This interaction has several important consequences: first, it leads to the formation of exciton states that are delocalized over both molecules in the ideal case (for the non-ideal case, see below). Second, the degeneracy of the excited-state energies of the non-interacting molecules is lifted and two exciton states form. The magnitude of the electronic Coulomb interaction $|V_0|$ determines the energy splitting between the exciton states, the so-called Davydov splitting, which is given by $2|V_0|$. Third, the TDM is redistributed to a specific exciton state, and this redistribution depends very sensitively on the mutual arrangement of the building blocks. Since only exciton states carrying TDM contribute to absorption and emission of light, this structural arrangement thus determines the photophysics of the dimer.

If the molecules are arranged face-to-face and thus the molecular TDMs are parallel with respect to each other, their Coulomb interaction is positive, $V_0 > 0$, and they form an H-aggregate (figure 1(a)). In this case, only the higher-energy exciton state is optically allowed and can absorb light. After light absorption rapid sub-picosecond relaxation into the optically forbidden lower-energy exciton state occurs (Kasha's rule), and therefore perfect H-aggregates are entirely non-emissive. The second extreme arrangement of molecules (and thus of molecular TDMs) is head-to-tail. Then the Coulomb interaction is negative, $V_0 < 0$, and a perfect J-aggregate forms (figure 1(b)). Here, only the lower-energy exciton state is optically accessible. This state is exclusively responsible for light absorption and emission. Moreover, the radiative rate of this lower-energy, emitting exciton state of a J-type dimer is increased by a factor of 2, i.e., by the number of interacting molecules. This state is referred to as super-radiant with a shorter lifetime compared to the excited-state lifetime of non-interacting molecules.

Other mutual arrangements of molecules, that are relevant in the context of this review, fall in between a face-to-face and a head-to-tail geometry. Those dimers can be understood by starting from the face-to-face arrangement and introducing a slip, or parallel offset, along the axis of the molecular TDM (often coinciding with the long molecular axis) until the head-to-tail situation is reached (figure 1(c)). Changing the slip angle θ between the molecular TDMs and the interconnecting axis from 90° (face-to-face) to 54.7° the Coulomb interaction V_0 is positive, $V_0 > 0$, but continuously decreases. In this angle range the dimer is of H-type although with an increasingly smaller exciton level splitting compared to the ideal face-to-face arrangement. At an angle of 54.7° the Coulomb interaction in point-dipole approximation vanishes, $V_0 = 0$, i.e., the molecules do not interact and no exciton states are formed. Towards still smaller angles, V_0 becomes negative, $V_0 < 0$, and its magnitude increases towards 0° (head-to-tail), i.e., we have a J-type dimer for this range of angles.

The extension of this dimer model to supramolecular nanostructures with $N \gg 1$ molecules is straightforward. For details, we refer to a recent review on that topic [17]. Briefly, instead of a doublet of exciton states for the dimer, in a large nanostructure a band with N non-degenerate delocalised exciton states forms. The band width W (energy difference between highest- and lowest-energy exciton) is also related to the magnitude of the electronic Coulomb interaction between molecules and is now $W = 4|V_0|$, which is often referred to as *free exciton band width*. In H- (J-) aggregates the optically allowed exciton states reside at the top (bottom) of the band, i.e., an H- (J-) aggregate is non-emissive (super-radiant), as discussed above.

Staying in the Kasha-picture, but providing a more realistic description of nanostructures, we must include electronic and structural disorder. Electronic disorder is caused by varying electrostatic interactions between the building blocks and their local surrounding. These interactions randomly shift the transition (site) energy of each molecule by ΔE around the mean value E_0 (the so-called diagonal disorder, according to its appearance in the exciton Hamiltonian). A non-perfect spatial assembly of the building blocks as well as (acoustic and optical) phonon modes of nanostructures give rise to (dynamic) variations ΔV of the electronic Coulomb interaction around the mean V_0 (the so-called off-diagonal disorder). The presence of disorder has two main consequences: first, for H-aggregates the emission becomes weakly allowed (sub-radiant), while in J-aggregates the super-radiant emission rate decreases. Hence, a disordered H- (J-) aggregate possesses a shorter (longer) excited-state lifetime compared to an ideal H- (J-) aggregate. Second, excitons are in general no longer delocalized across the entire assembly, but become increasingly localised on parts of the nanostructure. As long as $|V_0| \gg \Delta E$ (*strong-coupling limit*), the description of electronic excitations in terms of largely delocalized excitons is still a good approximation. Since this delocalization implies a coherent sharing of excitation energy between all molecules involved, this is often referred to as the regime, where *coherent energy transport* takes place. In the opposite situation $|V_0| \ll \Delta E$ (*weak-coupling* or Förster limit), electronic excitations are localized on individual molecules, and excitations are transferred according to Fermi's golden rule by *incoherent hopping* processes mediated by the (weak) electronic interaction $|V_0|$.

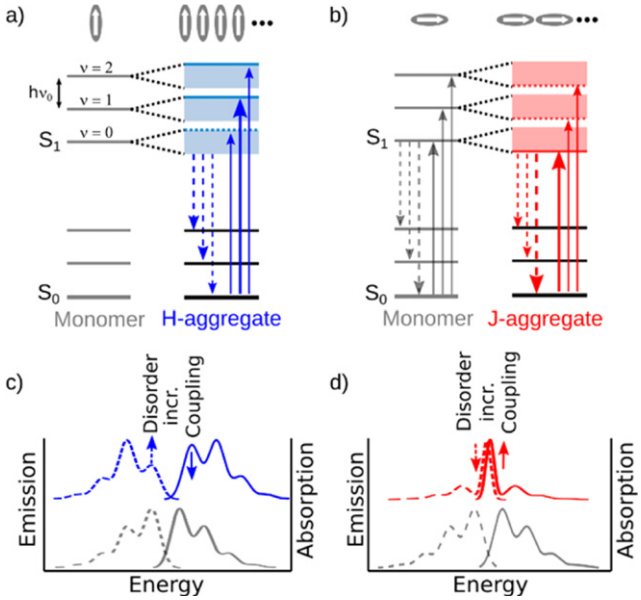

Figure 2. Spano model of interacting molecules including intramolecular vibrations coupling to the monomers' electronic states. (a) and (b) Energy level schemes for H- and J-aggregates with their series of vibronic exciton bands characterised by the vibrational quantum number ν. Optically allowed vibronic exciton states are at the top (H-aggregate) and bottom (J-aggregate) of each vibronic exciton band, respectively. (c) and (d) Absorption (solid) and emission spectra (dashed) of the non-interacting monomer with a typical vibronic progression (grey) and of H- (c) and J-aggregates (d), respectively, with their distorted vibronic progressions. Characteristic changes of relative peak intensities for increasing electronic Coulomb coupling and electronic disorder, respectively, are indicated by arrows for the absorption and emission spectra.

A further complication arises because the optical spectra of non-interacting organic functional molecules usually feature vibronic progressions that stem from electron–phonon coupling mainly to carbon-bond stretch vibrations with energies around $h\nu_0 \approx 1500\ \mathrm{cm}^{-1}$ (figure 2). If the electron–phonon coupling strength (more precise: the relaxation energy E_{rel} associated with this electron–phonon coupling) is of the order of or larger than the free exciton band width W, a modification of Kasha's picture is required. This was recently put forward by Spano and co-workers [18, 19] and uses a multi-particle basis set introduced in earlier work by Philpott [25]. In this picture, which we refer to as 'Spano-picture', the electronic interaction V_0 splits each excited state vibrational level of the non-interacting molecule into a manifold of delocalized vibronic excitons, i.e., excitons that are dressed by an intramolecular vibration and are characterized by the vibrational quantum number ν. These vibronic exciton band widths are reduced compared to the free exciton band width due to electron–phonon coupling. Moreover, the vibronic progression of the optical spectra becomes strongly distorted: absorption in H-aggregates takes only place into the highest-energy vibronic exciton state of each manifold, while all bottom states are optically forbidden. Notably, the transition into the highest exciton state of the lowest-energy ($\nu = 0$) manifold is suppressed with respect to that of the ($\nu = 1$) manifold (figure 2(c)); the intensity ratio of these transitions is directly related to the electronic interaction V_0 between building blocks. The emission, which occurs according to Kasha's rule from the lowest-energy exciton state in the ($\nu = 0$) manifold, is modified as well. The transition into the vibrationless ground state (0–0 transition) is forbidden for an ideal aggregate, whereas transitions into ground state vibrational levels are still allowed. The presence of disorder (in the limit $V_0 \gg \Delta E$) has only minor influence on the shape of the absorption spectrum. In emission, however, disorder renders the 0–0 transition weakly allowed, and its relative strength is related to the energy disorder ΔE. In J-aggregates the reverse situation is observed: the bottom vibronic exciton states in each manifold are optically allowed with the bottom state of the ($\nu = 0$) manifold being super-radiant. In absorption, the transition into the ($\nu = 0$) exciton manifold increases with V_0. Upon increasing disorder ΔE, in emission the super-radiant 0–0 transition is reduced in intensity. Combining information from absorption and emission spectra therefore allows to fully characterize the electronic parameters, photophysics and excited-state energy landscapes of supramolecular nanostructures.

The discussion so far included exclusively the electronic Coulomb interaction V_0 between the molecules' TDMs, which is a rather long-range, through-space coupling. Particularly in dense face-to-face or slightly slipped face-to-face arrangements, superexchange interactions mediated by overlap of ground and excited state

wave functions (HOMO–HOMO and LUMO–LUMO overlap[3]) can be substantial, too. This latter short-range interaction facilitates dissociation of neutral excitons into charge-transfer (CT) states with electrons and holes being located on adjacent molecules. In the perturbative limit[4], this charge transfer can be described by an effective short-range interaction V_{CT} comprising electron and hole transfer integrals as well as the energies of a molecule's excited state and of the CT state [26, 27]. In recent years, mainly Spano and co-workers extended and generalised the exciton theory to include those superexchange interactions [26–30]. In the limit of a pure CT aggregate, i.e., vanishing Coulomb interaction $V_0 = 0$, the sign of V_{CT} determines the type of the aggregate, e.g. $V_{CT} < 0$ yields a J-type CT aggregate. Importantly, J- and H-type CT aggregates feature identical spectral features as discussed above and shown in figures 2(c) and (d). The mutual arrangements of the molecules within a CT aggregate, however, can be entirely different from those within conventional, 'Kasha-type' aggregates (figure 1(c)). Since the sign of V_{CT} is determined by the sign of the electron and hole transfer integrals, which in turn are determined by the nodal patterns of HOMO and LUMO (see e.g. figure 4 in reference [26]), already small slips along a molecular axis can result in a sign change of V_{CT}. In other words, J-type behaviour can be observed for arrangements close to a face-to-face packing, for which the Kasha picture (based on Coulomb interactions only) predicted an H-aggregate. The term 'J- and H-type behaviour at unconventional (non-Kasha) packing geometries' [26] has been coined for this behaviour. In general, both long-range Coulomb and short-range superexchange interactions must be considered. This situation gives rise to interesting effects caused by interference between both interaction terms. For instance, assuming $V_0 > 0$, an H-aggregate in the Kasha-/Spano-picture results. This H-aggregate behaviour can be 'amplified' by a positive V_{CT}, i.e., the lowest energy absorption is further suppressed in the presence of CT-mediated short-range interactions (see figure 2(c)). In the opposite case, if V_{CT} is negative and dominates, $|V_{CT}| > |V_0|$, the aggregate will show overall J-type photophysics (compare figure 2(d)). To describe such aggregates, a two-letter notation was introduced, in which the first letter indicates the type based on the Coulomb interaction and the second the type derived from the CT-mediated interaction; an upper-case letter indicates the dominating interaction. The two examples in this paragraph are thus termed hH- and hJ-aggregate, respectively.

We close this section by a few words of caution: the weak and strong coupling regimes in the Kasha and Spano pictures have different definitions. Whereas in the Kasha picture the ratio $|V_0|/\Delta E$ is relevant, as discussed above, in the Spano picture the ratio W/E_{rel} is used to distinguish those regimes. In the latter picture, the situation depicted in figure 2 is thus the weak coupling regime with $W/E_{rel} < 1$, although strongly delocalized collective vibronic exciton states are formed. For further details, see e.g. reference [19]. Moreover, the initial classification of assemblies into H- and J-type aggregates historically stems from the hypsochromic and bathochromic spectral shifts with respect to the non-aggregated molecular building blocks for H- and J-aggregates[5], respectively. However, such classification according to spectral shifts is not reliable, because the gas-to-crystal shift can exceed spectral shifts induced by electronic Coulomb interactions [19]. Only the sign of the Coulomb (and CT-mediated) interaction, which depends on the mutual molecular arrangement, or the relative changes in spectral peak ratios, as outlined above, allow to distinguish H- and J-aggregates unambiguously.

2.2. Design and photophysical properties of functional supramolecular nanostructures

The section above discussed spectral features in the absorption and emission if two molecules or arrays of molecules assemble in a structurally distinct manner. Particular focus was given on how the excited-state energy landscape and the photophysical properties of supramolecular aggregates can be tuned by controlling the mutual arrangement of the building blocks. The basic control over this arrangement into nanostructures is achieved by the self-assembly of molecules via attractive, non-covalent secondary interactions. Those interactions include hydrogen bonding, ionic bonding, dipole forces and van der Waals forces or a combination of those, independent of the molecules' origin (i.e., natural or synthetic) and size (i.e., small molecules, oligomers or polymers). To achieve tailored functional nanostructures with defined shape, the self-assembly process is typically performed in liquid media and requires not only the presence of secondary interactions, but also a directionality of these forces. Consequently, suitable building blocks must be able to mediate beneficial secondary interactions by an appropriate design of the chromophore, the photoactive part of the molecule, as well

[3] By denoting ground and excited state wave functions as HOMO and LUMO we follow the convention in the literature. We note that it is beyond the scope of this work to address whether ground/excited state wave functions are appropriately represented by one-electron orbitals.

[4] In the perturbative limit, the energies of the exciton state and the CT state are non-resonant. In the resonant limit, those states are close in energy, which results in a complex two-band structure with two pronounced absorption bands [26,27].

[5] The term J-aggregate is named after Jelley, who observed in 1936 a red-shifted sharp absorption upon diluting a cyanine dye (1, 1′-diethyl-2, 2′-cyanine chloride) in non-polar solvents together with an strong increase in fluorescence [31]. Similar observations were made at the same time by Scheibe [32, 33].

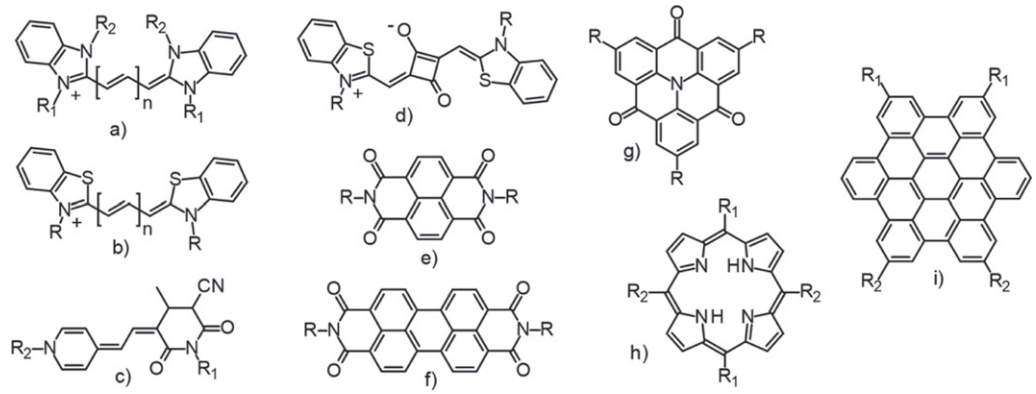

Figure 3. Commonly used conjugated organic chromophores together with typical substitution patterns (indicated by the non-specified substituent R, R_1 and R_2) for the formation of H- and J-type supramolecular aggregates. A large and diverse class of dyes are polymethines, which can be classified into several subclasses: exemplarily we show cationic cyanine-based core structures of (a) a benzimidacarbocyanine, (b) a benzothiazol cyanine (with $n = 0, 1, 2$, etc) as well as selected neutral or zwitterionic examples of (c) a merocyanine and (d) a benzothiazolium squaraine. Often used conjugated compounds feature also a more planar board- or disc-like structure such as (e) NDI, (f) PBI, (g) CBT, (h) porphyrins and (i) HBC.

as by appropriate peripheral substituents and substitution patterns. At the same time the chromophore design must take into account the desired function of the nanostructure, e.g. by tuning absorption into a specific spectral region.

This section is dedicated to provide examples of molecular species that self-assemble into distinct types of aggregates (J- or H-type), either in bulk or in solution, and demonstrates how a suitable molecular design allows to alter the type of aggregation (from J- to H-aggregate) using the same chromophore. We also show how distinct processing conditions allow to control the self-assembly of the same molecular species into either H- or J-type aggregates, or into different kinds of aggregates (e.g. two distinct J-type aggregates).

2.2.1. Self-assembly into H- and J-type aggregates by molecular design

One of the most interesting examples and design principles are nature's photosynthetic pigment-protein complexes, which are difficult to realise synthetically from scratch. Such sophisticated supramolecular systems require the preparation of macromolecules with extraordinary structural (i.e., configurational and conformational) precision and their specific self-assembly [16, 34]. For that reason, current research typically focusses on small molecules, which can be assembled into functional supramolecular nanostructures.

Most commonly, such building blocks form so-called supramolecular polymers, which are defined as '*polymeric arrays of monomeric units that are held together by highly directional and reversible non-covalent interactions, resulting in polymeric properties in solution and bulk*' [35, 36]. Supramolecular polymers are not limited to linear structures, but can also include two-dimensional or more complex architectures [37, 38]. Supramolecular polymers are also often classified in view of their objects' shape on the nano- and mesoscale such as nanoparticles (NPs), nanofibres (NFs), and nanosheets. In a wider sense, the term *supramolecular element* has been coined for such supramolecular objects [16].

Mechanistically, the growth of supramolecular polymers is categorized into isodesmic, cooperative and anti-cooperative mechanisms. Such kinetic aspects of polymer growth are not in the focus of this review. Here we refer to excellent reviews and essays dealing with considerations of supramolecular polymerization [36, 39–41].

In the context of this review, only supramolecular polymers or nanostructures are of interest, in which the excited-state energy state landscapes can be tuned. Investigating such structures by means of state-of-the-art optical microscopy and spectroscopy techniques, requires absorption and emission in the visible to near-infrared spectral region. Thus, the building blocks use chromophores, which are typically based on dye molecules or fused aromatics (see figure 3). The molecular design of the building blocks also considers a suitable substitution pattern of the chromophores for self-assembly and processing purposes. Well-investigated examples include molecules with a linear chromophore design such as the polymethine dyes [42]. A prominent class are cyanine dyes (figures 3(a) and (b)), which are typically present in a cationic form [43, 44]. Another important class of polymethine dyes are merocyanines [45] or squaraines [46] (figures 3(c) and (d)), which are present in neutral form or in its corresponding zwitterionic form. The latter two classes feature a pronounced dipolar (merocyanine) and quadrupolar character (squaraine), respectively, which results in a permanent dipole moment in merocyanines. Thus, these kind of molecules feature a donor–acceptor (D–A) [47]

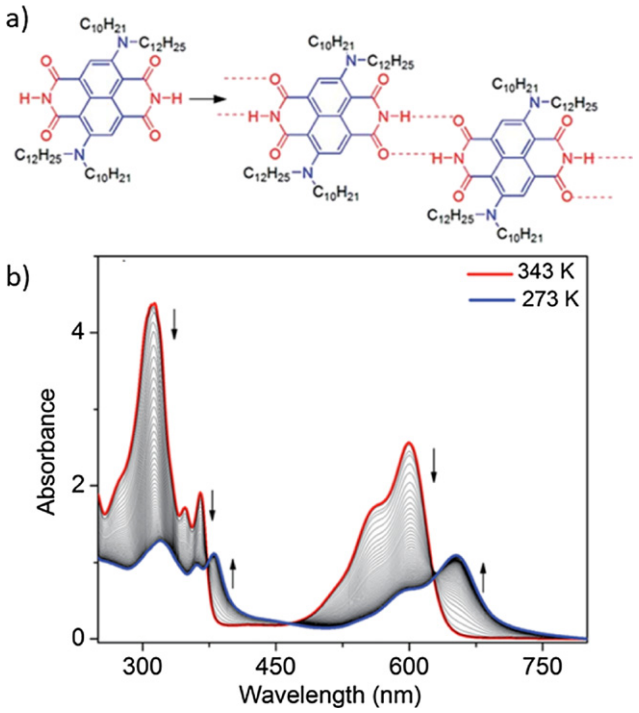

Figure 4. (a) Chemical structure of a core-substituted naphthaldiimde (NDI) with dialkyamino moieties (left) and the resulting supramolecular polymer featuring an ideal J-type arrangement (right). (b) In non-polar solvents, such as *n*-decane, gelation of the solvent due to supramolecular polymerization of NDI into J-aggregates takes place, which can be observed by the characteristic spectral changes upon cooling a 1.75 mM *n*-decane solution.Reproduced from [52]. CC BY 3.0.

or donor–acceptor–donor (D–A–D) [48, 49] structure, which strongly influences their aggregation behaviour and may give rise to CT states [50].

Besides those linear dyes, other often used chromophores comprise increasingly larger, mostly planar cores featuring a board-like to disc-like molecular geometry. Prominent examples are based on naphthaldiimides (NDI) [51, 52], perylenebisimides (PBI) [53, 54]), carbonyl-bridged triarylamines (CBT) [55, 56], porphyrins (or related structures[6]) [57, 58] and hexabenzocoronenes (HBC) [59, 60]) (figures 3(e)–(i)).

Considering now the aggregation capabilities of the photoactive part of such building blocks, the chromophores require a close vicinity so that their TDMs interact and exciton states and bands are formed (figures 1 and 2). Starting with a simple picture, for very small aromatics such as benzene, a direct face-to-face (or π-stacking) arrangement of two molecules is disfavoured because π-stacking is considered as a repulsive interaction [61, 62]. As a result, they feature an edge-to-face arrangement due to the energetically preferred interaction of the hydrogen atoms with the π-electrons of the neighbouring benzene. In the crystalline packing, however, the situation may become different, because in the resulting herringbone arrangement additional interactions between the molecules occur, e.g. with the next-nearest neighbours. In contrast, in larger aromatic systems and/or in systems with locally different electron densities (due to heteroatoms in or donor or acceptor-type substituents on the aromatic core), a face-to-face arrangement is often observed. Depending on the building block, i.e., larger aromatic systems or more polar aromatic systems, such parallel arrangement can feature a parallel offset (often called slipped), tilted or rotated orientation with respect to each other. With an increasing slip angle θ varying from 0 to 90°, this give rise to a change of the photophysical signatures from a J-type to an H-type aggregate (see figure 1(c)).

Besides the type of aggregation, the molecular design also aims to improve and guide the self-assembly process to achieve supramolecular polymers and nanostructures from solution. This can be accomplished by introducing (i) further secondary interactions, (ii) tailored peripheral moieties and by (iii) symmetrical substitution patterns. As attractive secondary interactions, hydrogen bonds are typically employed. Proper positioning of hydrogen bonding moieties enhances the capability of the building blocks to achieve a controlled self-assembly and, more importantly, these hydrogen bonding moieties can guide the self-assembly to a specific mutual arrangement of the chromophores. As peripheral substituents mostly large and flexible

[6] Structurally very similar molecules are chlorins and bacteriochlorins, which differ from porphyrin by omitting one or two double bonds in the five-membered rings. Both compounds are the basis of natural light-harvesting systems [42].

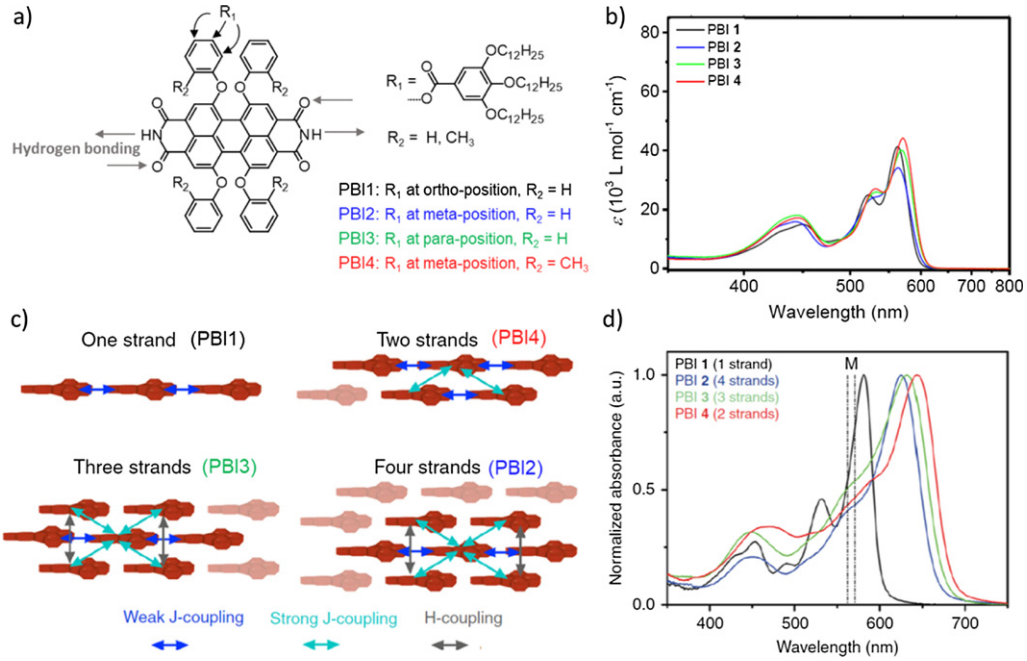

Figure 5. (a) Chemical structure of four different PBIs with each PBI bearing four bulky substituents in the bay region of the chromophore. Structurally, the different PBIs vary by the position of R_1 at the ortho-, meta- or para-position at each of the phenoxy-groups linked to the PBI and by the variation of R_2. (b) Absorption spectra of the molecularly dissolved PBI1-4 in dichloromethane featuring a very similar signature with maxima at 562–570 nm (note the non-linear wavelength scale). (c) In the solid-state the four PBIs feature a distinct aggregation behaviour: each PBI forms a strand reflecting an ideal J-type arrangement. For PBI2-4 different hierarchical arrangements of the strands exist giving rise to different interaction behaviour between the strands. (d) Normalized solid state absorption spectra of the aggregated PBI1-4 (M refers to the maxima of the molecularly dissolved PBIs). While self-assembled PBI1 features a slight red-shift reflecting an ideal J-aggregate, the spectra of self-assembled PBI2-4 are significantly red-shifted with respect to PBI1-based strands. In these multi-stranded structures additional J-type interactions (and one H-type interaction for PBI4) are present with the coupling being stronger between strands than along a strand. Reproduced from [66]. CC BY 4.0.

aliphatic moieties are employed with the primary aim to improve the solubility and thus the processing of the building blocks. Moreover, the use of aliphatic peripheral groups provides the opportunity to introduce chiral groups, a common tool utilized in supramolecular chemistry to investigate the aggregation process via circular dichroism (CD) spectroscopy [63, 64].

For the numerous different building blocks based on the chromophores mentioned above (figure 3), J-aggregates as well as H-aggregates are known, although some molecules (e.g. PBI, porphyrin and HBC) preferably form J-aggregates [40, 42, 59, 65]. In the following we give selected examples of building blocks, which are known to form one specific type of aggregate.

A simple, but efficient design principle is provided by Gosh *et al* using naphthaldiimde (NDI) as chromophore and bulky dialkyamino moieties in the periphery of the core for the supramolecular polymerization (figure 4(a)) [52]. Solutions of the molecularly dissolved core-substituted NDI in *n*-decane feature π–π^* transitions at 300–450 nm and an intramolecular CT transition at about 500–600 nm (figure 4(b), red). Upon aggregation, which can be achieved either by increasing the concentration or reducing the temperature, the dissolved NDIs start to form strands of hydrogen-bonds between the imide groups (figure 4(a)). This assembly results in a supramolecular polymer with a head-to-tail arrangement, which represents probably the ideal form of a J-aggregate (compare figure 1(b)). Indeed, the appearance of red-shifted absorption bands compared to the absorption of the non-aggregated NDI indicates the formation of J-aggregates (figure 4(b), blue). The J-type aggregation was confirmed by the observation of a super-radiant decay with a short inverse decay rate of about 45 ps.

A similar approach was pursued by the Würthner group [66]. They used PBI as chromophore, which represents the larger conjugated relative of NDI, and substituted the chromophore with four bulky phenoxy-based substituents at the bay region (figure 5(a)). Four different PBIs (PBI1-4) were synthesised, which mainly varied in the form of the sterically demanding side groups and in the position where those are attached to the phenoxy group. These substitution patterns do not significantly alter the optical properties of the chromophore as evidenced by the absorption of the molecularly dissolved building blocks (figure 5(b)). In the crystalline or liquid crystalline state, the PBI building blocks form a hydrogen bond pattern in a similar manner as described in the case of the NDI above. For PBI1, single strands with an ideal head-to-tail arrangement of the chromophores

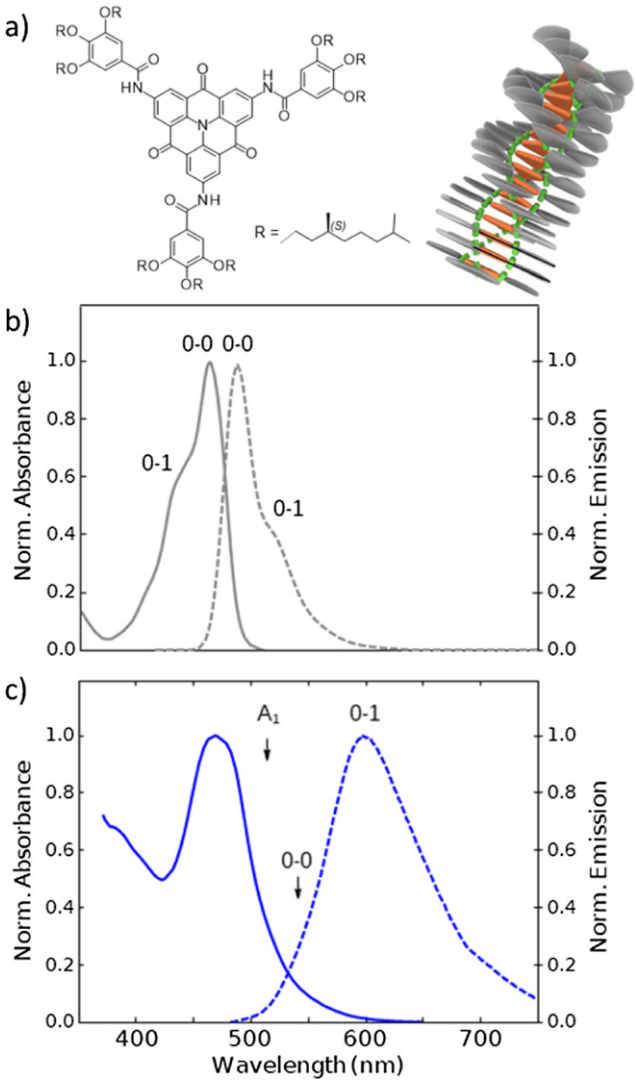

Figure 6. (a) Chemical structure of 2, 6, 10-substituted CBTs with three 3, 4, 5-tri-(3, 7-dimethyloctyloxy)benzoic acid amide side groups and their face-to-face arrangement due to the directed threefold hydrogen bond pattern (green dotted lines). Reprinted with permission from [56]. Copyright (2016) American Chemical Society. (b) Absorption (grey solid) and emission (grey dashed) of the molecularly dissolved building block in tetrahydrofuran, featuring a clear vibronic progression. (c) In non-polar solvents such as *n*-dodecane almost perfect H-type aggregates were formed featuring a distorted vibronic progression in both absorption (blue solid) and emission (blue dashed). A_1 indicates the absorption into the lowest energy vibronic exciton state. This H-type aggregation is evidenced by the absence of the 0–0 transition in emission. Compare reference [68].

form (figure 5(c)). The J-type aggregation is clearly visible by the red-shift, by the slight line-narrowing as well as by the more pronounced electronic (longest-wavelength) transition in the absorption spectrum of this single stranded structure (figure 5(d), black) compared to the absorption of the monomer (figure 5(b), black). The variation in the molecular design gives further rise to an aggregation at different hierarchical levels, including structural arrangements with 2 to 4 strands of the hydrogen-bonded PBIs (PBI2-4). Within this multiple-stranded structures the PBIs feature a slipped arrangement with respect to each other (figure 5(c)). The absorption of those hierarchically aggregated structures feature a clear red-shift compared to the monomer absorption (figures 5(b) and (d)). This red-shift is also significantly stronger compared to the single-stranded structure, which is caused by additional J-type interactions between the different strands within a hierarchical structure. Those additional interactions, indicated by cyan arrows in figure 5(c), are stronger than the head-to-tail interaction (blue arrows in figure 5(c)) due to the shorter centre-of-mass distances between the 'slip-stacked' PBIs as compared to the head-to-tail interaction. In the case of the three- and four-stranded structures an H-type coupling between the next-nearest strands becomes possible, as indicated by the black arrows in figure 5(c). This H-type interaction effectively reduces the J-type coupling and thus gives rise to a slight blue-shift of the three- and four-stranded structures compared to the double-stranded structures of PBI4. Note that the absorption spectra of PBI 2–4 feature also a significant broadening of the spectra compared to the single-stranded PBI1. This is indicative of a more pronounced (electronic and/or structural) disorder

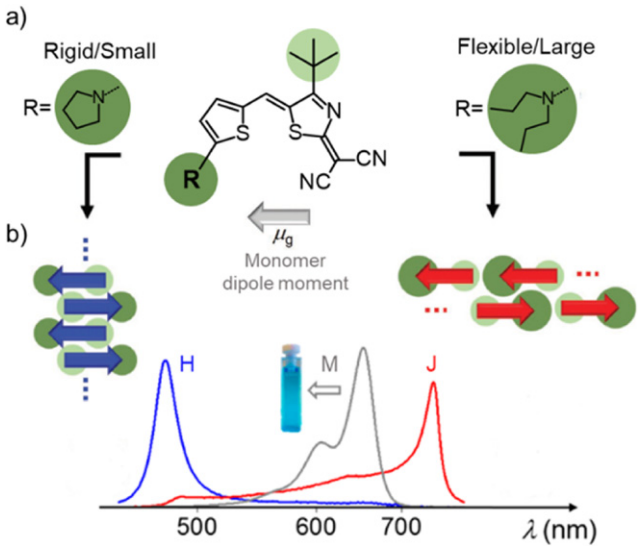

Figure 7. (a) Chemical structure of a merocyanine derivative with a tert-butyl group and either a pyrrolidine (left) or a di-*n*-propyl-amino substitution pattern (right). Reprinted with permission from [47]. Copyright (2016) American Chemical Society. (b) This small change in the peripheral side group results in different crystalline packings in the solid state featuring either a blue-shifted H-type or a red-shifted J-type signature in the absorption spectrum. M refers to the monomer absorption in solution. [69] John Wiley & Sons. [Copyright © 2019 WILEY-VCH Verlag GmbH & Co. KGaA, Weinheim].

within and between the individual strands. Those data clearly show how self-assembly of selected building blocks allows to tune the excited-state energies of the resulting supramolecular structures.

Going away from J-type aggregation towards an ideal face-to-face H-type arrangement, this can be achieved by self-assembly of a C3-symmetrically substituted building block featuring a slip angle of 90° (compare figure 1). A straightforward example of such a building block is based on CBT, a largely disc-like planar chromophore. CBT can be C3-symmetrically substituted close to the chromophore with three hydrogen-bonding amide groups, to which further bulky peripheral substituents are linked (figure 6(a)). This substitution pattern effectively suppresses the chromophore–chromophore slipping and ensures face-to-face arrangements. The ease of aggregation is demonstrated by the gelation of the solvent o-dichlorobenzene at very low concentrations (e.g. 7×10^{-3} M) [67].

In a more polar solvent, such as tetrahydrofuran, the building block is molecularly dissolved at room temperature, featuring a vibronic structure with maxima in the absorption and emission at 460 and 490 nm, respectively (figure 6(b)). Applying an elaborated self-assembly protocol, e.g., cooling a hot solution from *n*-dodecane, results in the formation of NFs with a face-to-face arrangement of the CBT-chromophores. This aggregation leads to significant changes in the shape of both the absorption and the emission compared to the dissolved building blocks (figure 6(c)). In particular, the suppression of the longest- (shortest-) wavelength peak in absorption (emission) clearly demonstrates an H-type aggregation, which is a result of the directed threefold hydrogen bond pattern. Remarkably, these NFs feature an almost perfect H-type optical signature as evidenced by the absence of the 0–0 transition in the emission spectrum compared to the molecularly dissolved building block (figure 6(c)) [68]. Those spectra are also an intriguing example of how the general expectation with respect to spectral shifts can be misleading in the assignment of the type of aggregation: upon self-assembly the emission maximum red-shifts substantially from 490 nm to 600 nm. This red-shift is determined by the gas-to-crystal shift, i.e., by the change in the local polarisable environment when going from molecularly dissolved CBT (solvent as environment) to NFs (highly polarisable conjugated CBT cores as next neighbours, see section 2.1).

The above mentioned examples demonstrate that proper positioning of hydrogen-bond forming moieties in NDIs, PBIs and CBTs lead to distinct types of aggregates, i.e., J- or H-type aggregates. One of the rare examples how the type of aggregation can be altered by a systematic variation of the molecular design is given by Würthner *et al* [47, 69] using essentially the same chromophore. The authors have employed distinct merocyanines, a chromophore featuring a substantial permanent dipole moment, which is the main driving force for the self-assembly process (figure 7(a)). Using selected side groups in the periphery results either in H- or in J-aggregates in the solid state. While the molecularly dissolved mercyanines have their absorption maxima at 650 nm with a pronounced vibronic progression, molecules featuring small aliphatic or rigid peripheral groups yield a stacking (H-type) arrangement of the chromophores with the absorption blue-shifted to about 480 nm (figure 7(b)). In contrast, larger or sterically demanding peripheral side groups induce a head-to-tail (J-type)

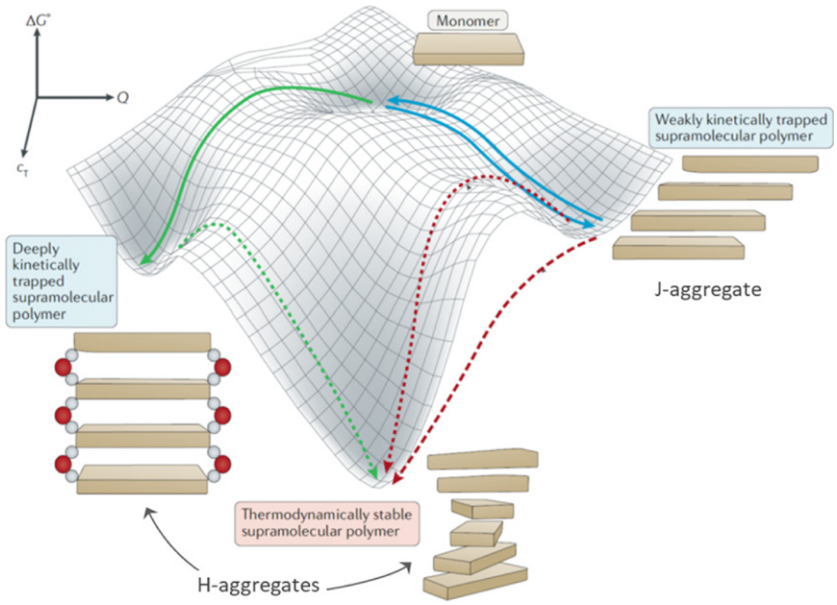

Figure 8. Schematic representation of a free energy landscape for the self-assembly of building blocks (monomers) from solution at different concentrations (c_T, total concentration) with various pathways to supramolecular polymers featuring different kinetically metastable or thermodynamically stable forms of aggregates. ΔG refers to the Gibbs energy and Q denotes the lowest-energy pathway along a set of geometry coordinates at a given concentration.Reprinted by permission from Springer Nature Customer Service Centre GmbH: Springer Nature [40] (2020).

arrangement of the chromophores, resulting in a red-shift of the absorption to 750 nm. For both the H- and J-type aggregates the vibronic progression is substantially less pronounced, indicating a very strong nearest-neighbour interaction due to the small nearest-neighbour distances within the solid-state. Effectively, these subtle changes in the design lead to a different steric demand of the molecules and thus to a different packing motif in the crystalline state. Remarkably, the photophysical properties are very different with the absorption being shifted nearly across the entire visible range [47, 69], demonstrating the potential of molecular design towards various optoelectronic applications requiring distinctly different spectral response.

2.2.2. Supramolecular nanostructures via pathway complexity

In addition to the aspects of molecular design discussed in section 2.2.1, selected solvents allow for the self-assembly of the same building block into nanostructures featuring a distinct type of aggregates. For instance in solution, a parallel aromatic stacking of conjugated chromophores can additionally be driven by preferred interactions between the solvent molecules, while the aromatic cores avoid contact with the (polar) medium [61]. This illustrates the delicate interplay between the building blocks and the chosen solvent. Similar observations were made for other self-assembly parameters, such as concentration, temperature window and rate of temperature change, and ageing, leading to the generally accepted conclusion that the processing conditions are of paramount importance for the self-assembly process.

Most notably, this situation becomes more complex, if kinetic and thermodynamic considerations allow for the formation of nanostructures of different type (H or J) and kind (e.g. different J-aggregates) using the same building block and similar processing conditions (figure 8) [40]. In this situation, the self-assembly of a building block can be described by a potential energy landscape or free energy landscape[7] and proceeds via different pathways until different (local) energetic minima are reached. These different, potentially accessible pathways lead to various thermodynamically stable and kinetically metastable supramolecular architectures. For the latter, the activation energy, which is required to eventually transform one metastable structure into another structure, determines to which extent a supramolecular polymer is trapped in this state [70]. As figure 8 also indicates, the structures formed in the energy minima feature a different mutual arrangement of the chromophores. This includes a helical, tilted or slipped arrangement of the building blocks in the aggregated species. A common way to distinguish between these different arrangements is CD spectroscopy, which can be beneficially used with building blocks featuring chiral groups. This method also allows to differentiate nanostructures of different kind, but of the same type, and to distinguish between the thermodynamically stable and deeply

[7] The *free/potential energy landscape* should not be confused with the *excited-state energy landscape*. The former refers to the (hyper)space of the free energy (ΔG) in which energetic minima for differently stable (aggregated) species exist due to configurational/geometrical considerations (forming a reaction pathway, see also figure 5).

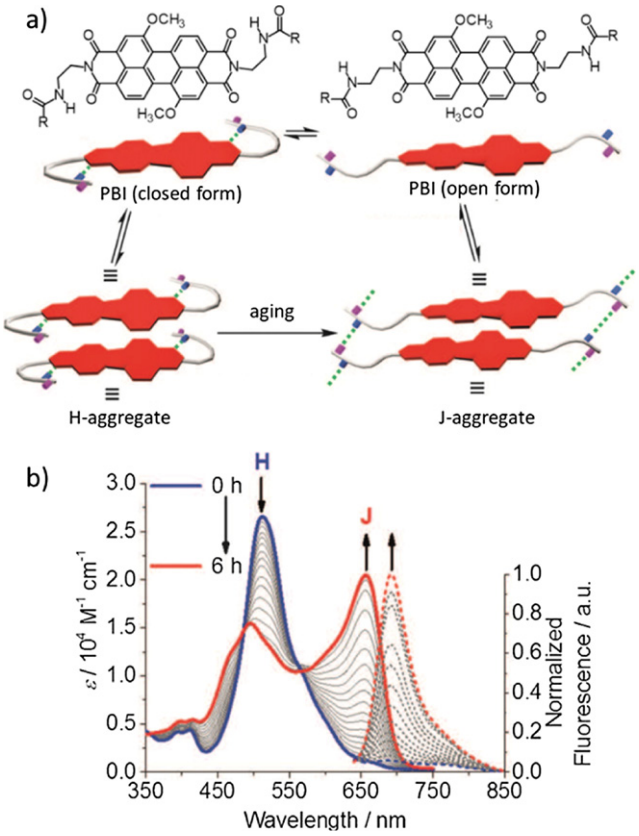

Figure 9. (a) Chemical structure and schematic sketches of H- and J-aggregates based on bay region-functionalized PBIs (R: 3, 4, 5-tridodecyloxybenzene). (b) H-aggregates form in a solvent mixture of methylcyclohexane and toluene (2:1, v/v) at a concentration of 15×10^{-6} M and a cooling rate of 5 K min^{-1}. Upon ageing at 20 °C, the H-aggregates transform via a rearrangement of the hydrogen bond pattern (indicated by the green dotted lines in (a)) into J-aggregates. [53] John Wiley & Sons. [Copyright © 2017 WILEY-VCH Verlag GmbH & Co. KGaA, Weinheim].

kinetically trapped species shown in figure 8. While both nanostructures represent an H-type aggregate, one of the structures exhibits chirality, which can be visualised by CD spectroscopy. This phenomenon, which is in general referred to as *pathway complexity* [40, 64, 70–72] yields nanostructures in solution that are based on the same building block, but show distinct (photo)physical properties and spectroscopic features. This behaviour goes often along with nanostructures of different morphology such as NFs, NPs or nanosheets.

For instance, Würthner *et al* demonstrated the use of a PBI derivative with an additional methoxy-substitution in the bay region of the chromophore and more importantly with an amide moiety decoupled by an ethylene group from the PBI (figure 9(a)). The latter allows for the formation of either an intramolecular hydrogen bond with the PBI chromophore (closed form) or an intermolecular hydrogen bond (open form) with an amide moiety on the neighbouring PBI. Self-assembly of the 'closed form' PBI results initially in a metastable H-aggregate, which can be achieved upon cooling dissolved PBI molecules from a solvent mixture of methylcyclohexane and toluene. The absorption of those H-aggregates is blue-shifted with respect to the monomer absorption (the monomer has its 0–0 absorption at 570 nm, not shown) and features the characteristic distorted vibronic progression with the suppression of the longest wavelength (lowest energy) absorption peak (figure 9(b), blue spectrum). Upon ageing, this aggregate is transformed within hours into the thermodynamically stable J-aggregate, which goes along with a strong increase in fluorescence. The J-aggregate exhibits a red-shifted absorption and dominant purely electronic 0–0 (highest wavelength/lowest energy) peak (figure 9(b), red spectrum). Structurally, the transformation to the J-aggregate is realized by the rearrangement of the hydrogen bonds from the intramolecular to the intermolecular pattern. This rearrangement of hydrogen bonds is accompanied by a slip along the long molecular axis to enter the J-type region of slip angles (compare figure 1(c)). Since the hydrogen bonding strand probably allow for a restricted slip only, this J-aggregate might be in an unconventional (non-Kasha) geometry; in this case the J-type photophysics would result from wavefunction overlap with concomitant pronounced CT interactions between adjacent, slightly slipped molecules (see section 2.1). Irrespective of the origin of the H- to J-type transformation, this example demonstrates the pronounced dynamic character in such self-assembled structures due to the secondary non-covalent interactions, a common feature in functional supramolecular polymers.

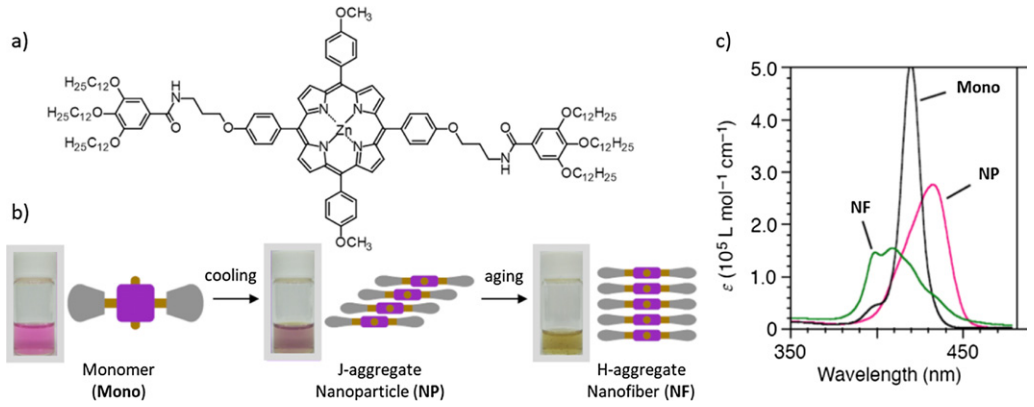

Figure 10. (a) Chemical structure of a Zn-porphyrin derivative with two bulky substituents, which can be molecularly dissolved in a hot methylcyclohexane solution. (b) Self-assembly of the building block upon cooling results in the formation of J-aggregates and may lead eventually to H-aggregates upon ageing. On the mesoscale, these J- and H-aggregates feature also different morphologies, such as NP and NF, respectively. (c) J- and H-aggregation were shown by the characteristic spectral (red- and blue-) shifts and changes of shape of the optical spectra. Reprinted by permission from Springer Nature Customer Service Centre GmbH: Springer Nature [73] (2017).

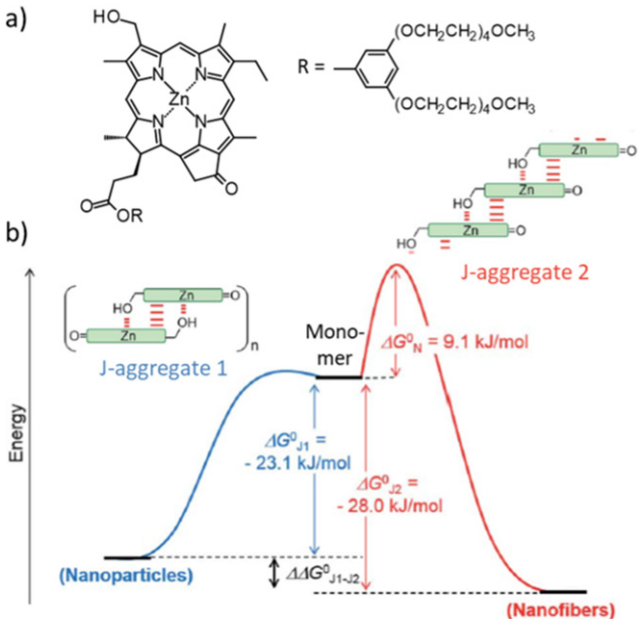

Figure 11. (a) Chemical structure of a semi-synthetic zinc chlorin derivative. (b) Schematic sketches of the metastable J-aggregate 1 with anti-parallel arrangement and the stable J-aggregate 2 with parallel arrangement of the building block. The corresponding free energy landscape indicates a higher activation energy for the more stable form. Reproduced from [75]. CC BY 3.0.

Another example of *pathway complexity* was reported by the groups of Takeuchi and Sugiyasu, showing that the self-assembly of distinct zinc porphyrin derivatives can lead either to a face-to-face (H-aggregate) or a brick-layer-type (i.e., slipped, J-aggregate) arrangement of the same molecules (figure 10) [57, 73, 74]. The absorption spectrum of the molecularly dissolved Zn-porphyrins features a maximum at about 420 nm. Upon cooling a hot solution using the non-polar solvent methylcyclohexane, selected derivatives form J-aggregates with a red-shifted signature in the absorption. On the mesoscale, this leads to the formation of kinetically trapped NPs. Upon ageing and stirring, the J-aggregates transform into thermodynamically more stable H-aggregates with a significant blue-shift in the absorption with respect to the monomeric species. Those aggregates form elongated NFs on the mesoscale. The authors also demonstrated that similar derivatives can rearrange on the mesoscale from NPs into 2D nanosheets [73].

A structurally closely related chromophore to the porphyrin is chlorin, which differs by omitting one double bond in the five-membered rings. In the semi-synthetic zinc chlorin derivative as shown in figure 11(a), however, the self-assembly leads to another structural arrangement of the chromophores as discussed for the Zn-porphyrins above. Here, *pathway complexity* during the self-assembly from methanol/water mixtures leads

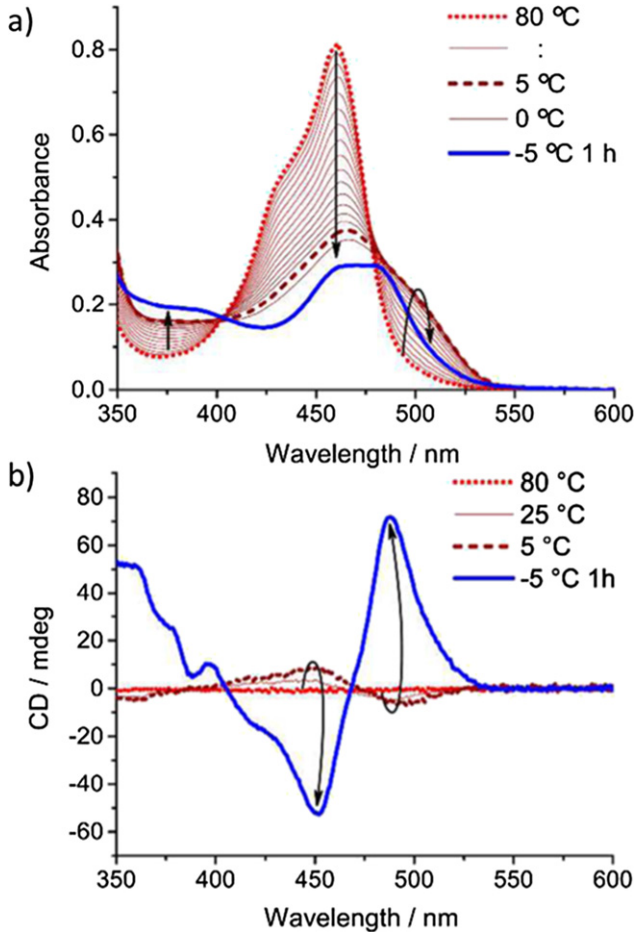

Figure 12. (a) Temperature-dependent UV–vis spectroscopy of the CBT derivative shown in figure 6(a) in the range of 80 °C to −5 °C in o-dichlorobenzene. (b) CD spectroscopy of the same compound using the same conditions revealing two different kinds of H-aggregates. Reprinted with permission from [56]. Copyright (2016) American Chemical Society.

to structure formation of the same type (i.e., H- or J-aggregate), but of different kind (i.e., only small changes in the structural arrangement). This is demonstrated by the formation of two different J-aggregates, a kinetically trapped J-aggregate (J-aggregate 1) and a thermodynamically stable J-aggregate (J-aggregate 2, figure 11(b)). Structurally, these aggregates differ by an anti-parallel and parallel arrangement of the chromophores, respectively. The kinetically trapped aggregate was found to be stable for months before it is transformed into its thermodynamically stable form [75]. In a similar manner as discussed for the porphyrin derivative above, this different packing gives rise to the formation of NPs or NFs on the mesoscale. The absorption spectra of both NFs and NPs exhibit the characteristic features of J-aggregates (red-shift with respect to the molecularly dissolved monomer and increase in relative intensity of the electronic peak). However, since the change in the molecular arrangement is only very small, these different kinds of J-aggregates are difficult to distinguish by linear absorption spectra, which are very similar in their shape and feature only very small spectral shifts with respect to each other. Here, CD spectroscopy was used to distinguish the different kinds of nanostructures by optical means.

An analogous finding was demonstrated using the CBT-derivative shown in figure 6(a), but here two distinct kinds of H-aggregates were found by applying selected self-assembly protocols [56]. In this case, o-dichlorobenzene was used as solvent that allows for dissolving the CBT building block at elevated temperatures as evidenced by the absorption spectra at 80 °C (figure 12(a)) featuring the same vibronic signature and maxima as shown before (figure 6(b)) as well as by the absence of a signal in CD spectroscopy (figure 12(b)). Upon cooling, self-assembly occurs as indicated by a change in the CD signal. Upon further cooling and ageing the CD signal changes drastically. The absorption spectra change as well, but always exhibit the characteristic shape of an H-type aggregate. Thus, under these conditions a kinetically trapped H-aggregate and a thermodynamically stable H-aggregate is formed. The former can be transformed into the thermodynamically stable aggregate by mixing both kinds of aggregates [56].

A similar finding was reported by Sanchez *et al* for building blocks based on CBT, where the amide moieties were moved away from the central CBT core by three ethinyl-phenyl spacers [76]. The formation of single

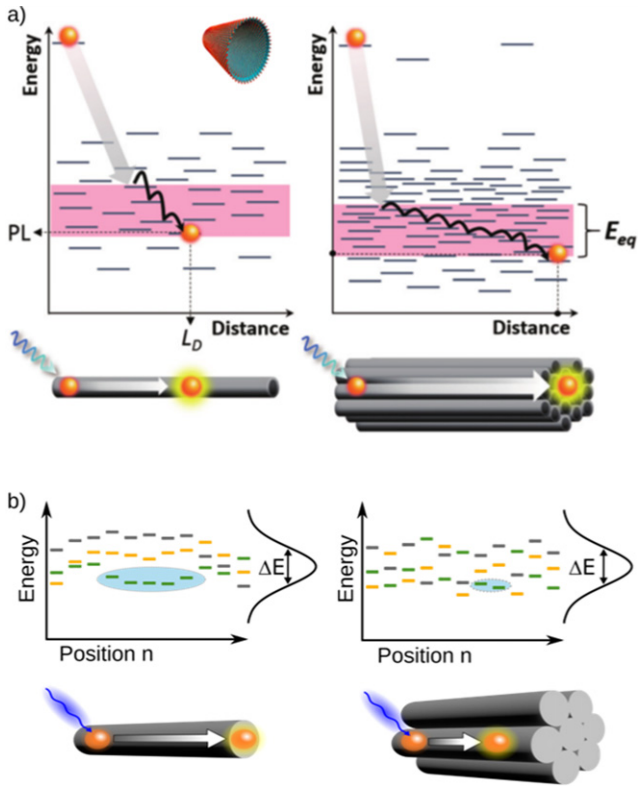

Figure 13. Tuning the excited-state energy landscape of supramolecular nanostructures by hierarchical self-assembly. (a) Excited-state energy landscape for supramolecular nanotubes (left) and bundles of nanotubes (right) based on the porphyrin derivative TPPS. The highest energy levels correspond to porphyrin's B-band into which excitation occurred, while the lower-energy levels are exciton states resulting from the Q-band. The red-shaded areas indicate the energy positions E_{eq} for relaxed excitons that are responsible for long-range transport along nanotubes or bundles of nanotubes. Reproduced from [87] with permission from The Royal Society of Chemistry. Reprinted with permission from [88]. Copyright (2017) American Chemical Society. (b) Three realisations of excited-state energy landscapes for single supramolecular NFs (left) and bundles of NFs (right) based on a CBT-derivative (figure 6(a)). Although the ensemble energetic disorder ΔE is identical for both hierarchical structures, the local energy landscape of each individual NF is significantly smoother in nanofibers due to spatially correlated site energies, giving rise to larger exciton delocalization and longer transport distances. Note that in (a) the disorder is presented in the excitonic basis, while in (b) this is in the site basis.

supramolecular NFs was demonstrated by AFM, and the absorption indicated H-type aggregation. Notably, using different solvents a thermodynamically and a kinetically trapped supramolecular polymer was found representing two kinds of H-aggregates [76]. Using similar building blocks, where the amide moieties were moved still further away from the central CBT core, the same group has demonstrated that kinetically trapped H-aggregates as well as thermodynamically stable J-aggregates can be formed [77].

Finally, another interesting and complex aggregation behaviour was observed by the research group of Belfield using a specially designed D–A–D squaraine dye in the presence of auxiliary materials in water [46]. The absorption maximum of the molecularly dissolved benzothiazolium squaraine dye (see figure 3(d), with R being a (pyridinium-1-yl)butyl cationic side group) was found to be at 643 nm with a concentration-dependent formation of a slightly blue-shifted dimer at 592 nm. Upon adding a small amount of a polyelectrolyte with an anionic backbone, i.e. poly(acrylic acid) sodium salt, a significant amount of an aggregated species was found demonstrating that the polyelectrolyte acts as template. Interestingly, time-dependent investigations reveal that initially an H-type aggregate with an absorption maximum at 560 nm was formed, which is transformed into a strongly red-shifted, well-organized, yet, 'non-fluorescent J-aggregate' with a maximum at 765 nm. Recently, Zheng *et al* [78] theoretically assigned this latter type of aggregate to a non-Kasha-type H-aggregate. In contrast to the aforementioned systems, showing different kinds of transformations of H-type and J-type aggregates, D–A–D squaraine-based systems resembles until now one of the rare examples for pathway complexity with a transformation from a Kasha-type H-aggregate into a non-Kasha-type H-aggregate.

Having shown that the type as well as the kind of an aggregate strongly depends on the molecular design and the selected processing conditions, it is probably not surprizing that the complexity of the self-assembly behaviour of a selected building block can be extended to include different types as well as different kinds of aggregates using proper self-assembly protocols [54, 79]. All these reports suggest, that the different supramolecular arrangements using small molecules require an extensive control of the self-assembly process to achieve supramolecular nanostructures with distinct properties.

Apart from the features of pathway complexity, the research activities in this field have also opened up new interesting avenues. For instance, the self-assembly of the selected PBI (figure 9), the porphyrins (figure 11), as well as distinct CBT derivatives were demonstrated to be suitable for living supramolecular polymerization [53, 74, 77]. In general, a living form of polymerization with active chain ends allows to achieve block or segmented structures within supramolecular nanostructures using two or more different building blocks. Although it seems that controlling the self-assembly into defined block copolymers is challenging to achieve [40], this has been already realized for selected PBI derivatives [80]. Such nanostructures are of fundamental interest to tailor exciton transport characteristics and to add novel functionalities to supramolecular nanostructures. First, different supramolecular building blocks possess different spectral characteristics (excited-state energies), and thus excitons experience distinct excited-state landscapes in the different blocks of the nanostructures. Second, in such architectures the different blocks are directly connected, i.e., there is an interface on the molecular scale comprising only two molecules, which allows to study interfacial processes in a well-defined arrangement.

3. Increasing complexity by hierarchical self-assembly: fine-tuning the excited-state energy landscape

3.1. Hierarchical supramolecular nanostructures: the impact of bundling

While the previous sections dealt with self-assembly into H- and J-type nanostructures determined by the molecular design of building blocks and processing conditions, here we expand this discussion towards hierarchical nanostructures. Hierarchical organization to larger objects covering all length scales is a common feature in nature that allows to tune and enhance material properties [81]. In this context, self-assembly into hierarchically structured supramolecular objects can be considered as the next higher level of aggregation beyond the supramolecular nanostructure [82–84]. More specifically, we refer here to hierarchical nanostructures as larger architectures that comprise (many) identical H- or J-type supramolecular nanostructures in bundle-like structures. Those bundles are formed using specific preparation protocols and possess different (photophysical) behaviour owing to their higher level of aggregation covering different length scales [85].

In recent years the potential of hierarchical structuring of artificial supramolecular systems emerged to fine-tune excited-state energy levels and to optimise e.g. energy transport or light-harvesting characteristics. A prominent and well-studied system represent J-type supramolecular nanotubes and bundles of nanotubes based on meso-tetra(4-sulfonatophenyl) porphyrin, TPPS (compare figure 3(g)). In its diacid form the self-assembly of TPPS into isolated nanotubes or bundles of nanotubes can be controlled in solution by changing the cation in added alkali chloride from Cs^+ to Na^+. In both cases, TPPS self-assembles into nanotubes with about 20 nm diameter (figure 13(a), inset), which can be envisioned as two-dimensional sheets rolled up into a tubular structure. Within a sheet's plane TPPS features a slipped-stacking in both perpendicular directions, and the porphyrin core is thus tilted out of plane by about 25° in both directions [86]. Upon bundling the resulting hierarchical structure has a diameter of some 100 nm. The slipped stacking of the TPPS molecules results in the formation of J-aggregates, which is confirmed by the red-shifted absorption of both the Q- and B-bands of porphyrin, which refer to the low- and high-energy absorption band, respectively. The PL spectra (only from Q-band) red-shift and become narrower for both the bundles and nanotubes compared to the Q-band emission of TPPS monomers [87].

Kim and co-workers compared the spectroscopic features of individual nanotubes with those of single bundles of nanotubes [87]. The bundles exhibit in general slightly broader spectral line widths and on average more red-shifted PL spectra with respect to single nanotubes. The authors concluded that in bundles the interactions between nanotubes leads to a larger degree of (electronic) disorder, to a denser distribution of energy levels in the excited-state landscape (figure 13(a)), and to an increased system–environment coupling. Usually, larger disorder is associated with a stronger localisation of excitons and less pronounced energy transport characteristics. However, a counterintuitive behaviour was observed: the coherence length (delocalisation) of relaxed excitons near the bottom of the exciton band (from Q-band) was nearly identical with about 2 nm in both cases, but the exciton mobility was substantially enhanced by bundling. Using direct steady-state PL-imaging (figure 14(a)) the diffusion lengths (diffusion constants) were measured to be relatively large with 370 nm (3.93 $cm^2\ s^{-1}$) in bundles and only 160 nm (0.95 $cm^2\ s^{-1}$) in nanotubes. It was speculated that in bundles the denser distribution of excited-state energy levels in combination with the stronger system–bath coupling facilitates thermally activated hopping of excitons. Thus longer transport distances can be achieved in bundles despite larger disorder (figure 13(a)). For bundles of TPPS-based nanotubes the diffusion coefficients as well as the short coherence lengths of relaxed excitons were independently confirmed by picosecond transient absorption microscopy measurements on individual bundles combined with theoretical modelling [88].

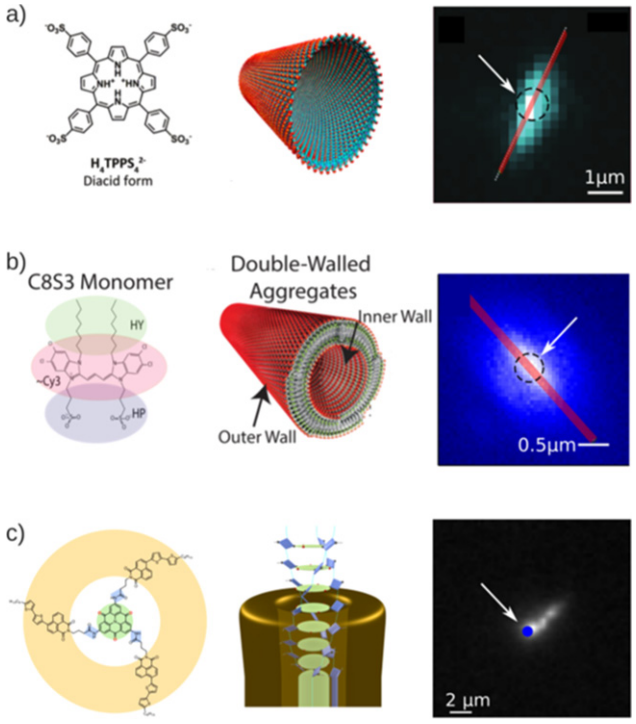

Figure 14. Direct photoluminescence imaging of long-range energy transport in single (hierarchical) supramolecular nanostructures. (a) Meso-tetra(4-sulfonatophenyl) porphyrin, TPPS, in its diacid form self-assembles into J-type tubular nanostructures. Right: PL image of a single bundle upon confocal excitation (black dashed circle). The red line indicates the long axis of the nanotube bundle. Reproduced from [87] with permission from The Royal Society of Chemistry. Reprinted with permission from [88]. Copyright (2017) American Chemical Society. (b) The cyanine dye C8S3 self-assembles into J-type bundles of double-walled supramolecular nanotubes. Right: PL image of a single bundle upon confocal excitation (black dashed circle). The red line indicates the long axis of the nanotube bundle along which long-range energy transport occurs. Reprinted with permission from [15, 94]. Copyright 2016 and 2014 American Chemical Society. (c) CBT, substituted with a bulky fluorescent periphery self-assembles into H-type NFs. Right: the PL image of a single NF upon confocal excitation (blue circle) shows an elongated PL profile along the NFs axis indicating efficient long-range energy transport. Reprinted by permission from Springer Nature Customer Service Centre GmbH: Springer Nature [55] (2015).

A further extensively investigated hierarchical system are double-walled nanotubes and bundles thereof that form by self-assembly of the amphiphilic cyanine dye C8S3 in aequous solutions (water/methanol mixtures, figure 14(b)). Note that we refer here to such a double-walled nanotube as a supramolecular nanostructure and a bundle of nanotubes represents a hierarchically structured object. A double-walled nanotube based on C8S3 is the simplest intrinsically achievable nanostructure (i.e., it represents the lowest level of aggregation) owing to the molecular design of C8S3 with its hydrophobic and hydrophilic interactions of the side groups appended to the cyanine building block. The self-assembly of C8S3 occurs into an extended herringbone arrangement [89]. The inter-wall electronic Coulomb interaction is relatively weak, of the order of some ten cm^{-1}, and allows only for incoherent hopping of excitons between the walls (of both isolated or bundled nanotubes) [90]. Within each wall the intermolecular Coulomb interaction is strong with magnitudes exceeding 1000 cm^{-1}, which favours formation of delocalised excitons [15, 91, 92]. The lowest-energy absorption and the emission lines of the (bundled) nanotubes are red-shifted with respect to the monomer spectrum, and the spectral lines are sharp with essentially no Stokes shift, which is characteristic of J-aggregates with very low degree of disorder [15, 91]. The slightly different packing of C8S3 molecules in the outer and inner wall, and the different radius of each wall lead to spectrally separate lowest-energy exciton bands, with the exciton band of inner wall being at slightly lower energy [43, 90]. In other words, each nanotube can be considered as a light-harvesting antenna structure, similar to those found in nature, since excitation energy is efficiently funnelled towards the inner wall [93].

Initial direct measurements of energy transport by static PL imaging of single structures yielded exciton diffusion lengths (constants) of 140 nm (1.2 $cm^2\ s^{-1}$) for isolated double-walled nanotubes and 790 nm (70 $cm^2\ s^{-1}$) for bundles (figure 14(b)) [94]. The optical spectra appear broader in bundles indicating a slightly larger degree of disorder as compared to isolated nanotubes, a similar trend as in TPPS-based structures discussed above. The large transport distances in bundles of C8S3-based nanotubes were proposed to originate from a large contribution of coherent transport, i.e., strongly delocalised excitons hop incoherently between extended coherent domains [94]. Indeed, theoretical modelling indicated substantial delocalisation of up to 1000 molecules [43]. Since energy is efficiently funnelled into the inner wall, which then probably contributes

most to long-range transport, it was proposed that the cylindrical structure and, in particular, the protection of the inner wall by the outer wall preserves favourable excitonic characteristics and thus limits perturbations of the inner wall upon bundling [43].

Very recently, we reported on hierarchically structured H-type architectures [68]. Using selected solvents, we self-assembled a CBT-based building block (figure 6(a)) into isolated supramolecular NFs or into bundles of supramolecular NFs. A combination of optical spectroscopy, numerical simulations and direct, time-resolved measurements of pico- to nanosecond energy transport dynamics, allowed us to gain insights into the relationship between hierarchical level, electronic (energy) disorder, and energy transport characteristics (figure 13(b)). While the overall (ensemble) energy disorder ΔE is very similar for NFs and bundles, we found that NFs feature spatial correlations of transition energies of adjacent CBT building blocks[8]. The presence of such spatial correlations gives rise to a segmentation of a nanofiber into local domains with a rather uniform excited-state energy landscape [95, 96]. This enables exciton delocalisation over >6 molecules and favours long-range energy transport over hundreds of nm with high diffusion constants of up to 1 $cm^2\ s^{-1}$. This diffusion constant measured for isolated NFs is, in fact, the highest reported for H-aggregated supramolecular nanostructures so far. In contrast, in bundles such spatial correlations are absent, which results in larger energy disorder between adjacent CBT molecules and localises excitons on < 2–3 molecules. As a consequence, diffusion constants in bundles are smaller by about one order of magnitude as compared to nanofibers. We ascribed those differences in the energy landscape and transport characteristics between NFs and bundles to a larger (local) electronic disorder induced by interaction of the large aliphatic side chains of CBTs self-assembled into bundles. Those interactions can destroy locally shared electronic environments of adjacent CBT cores, thus destroy correlations in transition energies, and ultimately render transport characteristics less favourable in bundles (figure 13(b)).

It is certainly a surprizing observation that in J-aggregates exciton transport appears to be enhanced upon bundling, while in H-aggregates the opposite behaviour is found. At present, we can only speculate about the reasons and whether this is a generic behaviour in J- and H-aggregates. Probably a complex interplay between the electronic/structural disorder, electronic coupling between monomers, and the supramolecular morphology upon self-assembly and bundling is important in this context. The specific molecular design of the building blocks can be a key factor as well. In particular, the chemical structure of appended side groups and their interactions upon bundling can play an important role.

The examples discussed in this section illustrate that hierarchical self-assembly provides ample opportunities to fine-tune energy landscapes towards optimising a desired functionality, such as energy transport or light-harvesting properties. However, the effect of hierarchical self-assembly can still not be understood in a straightforward way and is sometimes counter-intuitive as demonstrated by the observation of longer exciton diffusion lengths despite larger bundling-induced disorder in nanotubular systems. Further systematic studies in this direction are clearly required to be able to unleash the full potential of hierarchically structured nanosystems.

3.2. General aspects of long-range energy transport in (individual) supramolecular nanostructures

Here we extend the discussion from section 3.1 towards more general aspects of energy transport. We focus mostly on transport in single nanostructures, because a single-object approach allows for a direct study of transport properties beyond averaging over disordered ensembles.

While there is a plethora of photoactive, conjugated supramolecular building blocks that can be self-assembled into a variety of morphologies (see section 2.2), reports on nanostructures that support long-range energy transport of excitons along specific directions are still scarce. Here we consider transport as long-range if it occurs over at least 100 nm. This small number of studies may be related to several issues including (i) preparation of suitable nanostructures, (ii) their transfer to substrates, which may (iii) induce structural and electronic disorder, and (iv) photophysical considerations (kind and type of aggregates): in detail, self-assembly of the photoactive building blocks into highly ordered, well-defined, and sufficiently elongated nanostructures on the mesoscale is not always possible. Self-assembly is generally performed in solution resulting in colloidal dispersions with numerous objects. For investigations on single nanoobjects the supramolecular objects have to be transferred to substrates and/or have to be embedded into suitable matrices, where the individual objects must be well-separated from each other. This transfer should not introduce significant (structural and electronic) disorder. Moreover, it is unclear how the interplay between electronic Coulomb coupling and unavoidable (structural and electronic) disorder influences energy transport characteristics, and, in particular, whether

[8] Spatial correlations between site energies of neighbouring molecules are described by a correlation length l_0, expressed in units of molecules. For $l_0 = 0$ the site energy of each molecule is chosen independently from a (typically Gaussian) distribution with width ΔE (figure 13(b)), whereas an infinite l_0 means that site energies are identical for each molecule within one aggregate (but those are different for different aggregates in an ensemble of nanostructures). For a given energy disorder ΔE the exciton delocalisation increases with the correlation length [95, 96].

some degree of disorder is actually required for efficient long-range transport [97–99]. Finally, most energy transport studies have been performed on J-type systems, because their favourable super-radiant photoluminescence properties (high PL-signal) facilitate their imaging and spectroscopy. But nanostructures optimized for energy transport do not necessarily have to be good emitters [10]. H-aggregates with subradiant emitting exciton states can be better candidates for long-range transport due to the significantly suppressed competition between radiative decay and energy transport. This, however, renders spectroscopic measurements on single objects experimentally challenging.

To date supramolecular nanostructures based on chromophores, such as perylenes [100, 101], cyanines [15, 43, 94, 102, 103], phenanthrenes [104, 105], porphyrins [88], HBC [59] and CBT [55, 68] (see also figure 3), are reported to sustain long-range transport. These building blocks were self-assembled into elongated (hierarchical) nanostructures such as NFs, nanotubes and double-walled nanotubes. In those nanostructures, transport distances of some 100 nm, up to about 800 nm, have been demonstrated either by direct microscopic PL imaging (figures 14(a) and (b)) [88, 94, 100, 106], by indirect exciton–exciton annihilation [102] or sensitizing experiments [104, 105, 107]. Still longer transport distances were reported by Caram *et al* [15] who showed via annihilation measurements distances of (1.6 ± 1.0) μm in C8S3-based J-type double-walled nanotubes stabilised in a sugar-based matrix. We have recently reported exciton transport of more than 4 μm in single H-type supramolecular NFs based on CBT using direct PL imaging experiments (figure 14(c)) [55]. Such long-range transport is generally achieved by a combined coherent–incoherent transport mechanism. That is, excitons are delocalised across a nanostructure to some extend (depending on disorder, see sections 2.1 and 3.1) and thus the wavefunction of the molecules involved is coherently shared, which we refer to as coherent transport. Excitons perform incoherent hopping between such coherent domains, and the larger those domains are, the farther transport occurs with a single hopping step. Giuseppone *et al* reported on a further transport mechanism in supramolecular nanostructures based on triarylamine tris-acetamide [108]. This transport took place over more than 10 μm and was coined plasmonic transport, since it only occurred upon oxidation of the nanostructures.

Such μm-scale transport distances in densely packed nanostructures with typically sub-nm chromophore–chromophore distances indicate that more than 10 000 molecules can be involved. It is interesting to note that more than 80 years ago Scheibe[9] already described similar transport distances for supramolecular polymers based on cyanine dyes using quenching experiments [109]. Taking into account the typical excited-state lifetimes of excitons, i.e., tens of picoseconds in J-aggregates and some nanoseconds in H-aggregates, such transport distances translate into exciton diffusion constants from about 1 $cm^2\ s^{-1}$ [68, 88, 94] up to $\sim$50 $cm^2\ s^{-1}$ [15].

These long transport distances and high diffusion constants are rather surprizing for self-assembled organic structures with unavoidable electronic and structural disorder. It is even more surprizing considering that these transport distances of singlet excitons exceed those commonly observed in highly ordered organic single crystals[10] as well as in (semicrystalline) organic thin films by sometimes more than two orders of magnitude [111, 113–118]. The origin of these long distances in supramolecular nanostructures is not entirely clear yet and subject to on-going discussions [10], in particular, since micrometre transport has been demonstrated on both J- and H-type nanostructures. While for H-aggregates the long excited-state lifetimes of some nanoseconds favourably reduces the competition between decay and transport, for J-type structures the lifetime is typically tens of picoseconds only, which requires particularly fast and efficient transport characteristics. One factor common to those efficiently transporting nanostructures is a strong nearest-neighbour Coulomb interaction between the constituent molecules that can exceed 1000 cm^{-1} [15, 68, 91, 92]. Usually these couplings are determined in point-dipole approximation. If non-nearest neighbour interactions are accounted for as well, transport speeds up significantly due to stronger exciton delocalisation (coherent transport) and concomitant incoherent hopping between larger coherent domains [119]. In fact, in J-aggregates the point-dipole approximation underestimates the actual magnitude of this interaction, while in H-aggregates the actual interaction is overestimated [120]. This aspect can contribute to extraordinary transport properties and especially to the fast transport in J-aggregates with high diffusion constants. A further factor for fast, efficient and long-range transport is probably a low degree of structural and energetic disorder within a nanostructure [15, 68]. For instance, Caram *et al* concluded that the μm transport in their double-walled nanotubes results from a low (static and

[9] In 1937, Scheibe was apparently aware that the observed cyanine-based J-aggregates resembles what we nowadays call supramolecular polymers [33]. In 1939, he described those having a pretty clear picture: '*they are loose polymers of dye ions bound by van der Waals forces. The hydrophobic hydrocarbon moieties play an essential role in this bonding. Presumably, the flat dye molecules lie on top of each other like a roll of coins and thus form thread-like structures*' [109]. More astonishingly he described the photophysical behaviour with respect to the exciton transport as follows: '*the light irradiated into a molecule can be propagated extremely fast due to the coupling of the resonators, so that the light was nonetheless propagated over several 10 000 molecules [...]*' [109].

[10] We want to emphasise that we refer to transport of singlet excitons. Triplet transport in single crystals has been reported to occur up to several μm due to the usually long triplet exciton lifetime [110–112].

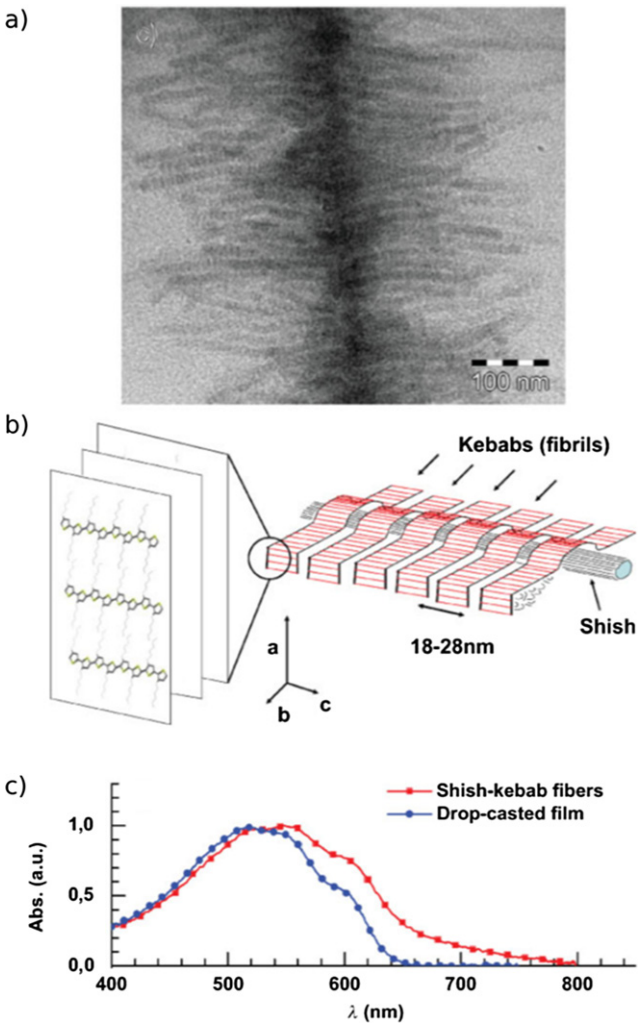

Figure 15. Shish–kebab superstructure based on epitaxial growth of the conjugated polymer poly(3-hexylthiophene), P3HT. (a) Brightfield transmission electron microscopy image. (b) Schematic illustration of the shish–kebab morphology: P3HT NFs (kebabs) with a lamellar width of 18–28 nm grow laterally away from the central P3HT-shish. The P3HT-NFs form by π-stacking of the polymer backbones. (c) Absorption spectra from shish–kebab NFs as well as from a drop-cast P3HT-film, confirming the H-type aggregation of P3HT by the suppressed longest wavelength absorption around 620 nm. [123] John Wiley & Sons. [Copyright © 2009 WILEY-VCH Verlag GmbH & Co. KGaA, Weinheim].

dynamic) electronic disorder [15], as verified later by Kriete *et al* by single-object spectroscopy [91]. This indicates a flat excited-state energy landscape with substantial exciton delocalisation contributing to long-range energy transport. We have recently demonstrated that spatial correlations in the transition energies of adjacent supramolecular building blocks along H-type CBT-based NFs provide a (locally) smooth excited-state energy landscape within each single NF (figure 13(b)) [68]. This contributes to a larger exciton delocalisation and thus enables faster, long-range transport as compared to nanostructures in which such correlations are absent.

Other factors for efficient long-range energy transport, however, remain still unclear: for instance, how the precise chemical structure of the supramolecular building blocks (torsionally flexible vs stiff and planar aromatic core) influences transport characteristics. The electron–phonon coupling to intra-molecular (low-energy) vibrational (torsional) modes and how this affects transport in supramolecular nanostructures is largely unexplored territory. Moreover, upon self-assembly of supramolecular building blocks the side-groups can arrange into either (partly) crystalline or entirely disordered structures. Highly ordered side group arrangements may be able to provide a shared local environment for several adjacent molecules within a nanostructure. At least on a local scale particularly well-defined, smooth excited-state energy landscapes may emerge, which is clearly favourable for transport characteristics. Finally, specific polarisable side groups appended to the supramolecular building blocks are known to shift the transition (site) energies of molecules. Upon self-assembly this can then influence the excited-state energy landscapes with potential impact on transport dynamics of excitons. Those questions remain to be investigated in future work.

3.3. Supramolecular complex superstructures

As demonstrated, hierarchically structured architectures provide a new level of complexity in tailoring the excited-state energy landscape in supramolecular nanostructures based on small molecules. This level of complexity within nanoscale-objects is further increased, if two (or more) distinct (hierarchical) supramolecular nanostructures are combined to a (composite) material, which we here refer to as complex superstructures. Superstructures or complex superstructures with dimensions on the nano- and mesoscale are interesting candidates, since potential applications of supramolecular architectures in optoelectronic and nanophotonic devices require control not only of their electronic and optical properties, but also efficient interfacing with other structures to connect with e.g. electrodes and contacts [121]. In this regard, supramolecular complex superstructures potentially provide an elegant way to achieve orientation and alignment of supramolecular nanostructures in a controlled and well-defined manner.

The first superstructure to be discussed in this section are so called 'shish–kebab' (micro)structures[11] formed by self-assembly of the conjugated polymer poly(3-hexylthiophene), P3HT. Brinkmann *et al* for instance used a large thread-like P3HT-structure (the 'shish'), which was initially nucleated on a 1, 3, 5-trichlorobenzene fibre-like structure. From this shish P3HT NFs (the 'kebabs') grow perpendicularly away (figure 15) [123]. While the central shishs had lengths of up to 100s of micrometres, the perpendicular P3HT kebabs were between 100 nm and 1 μm long and arranged in a highly oriented and dense fashion (figure 15(a)). Structurally, the P3HT NFs grow by π-stacking of the conjugated backbone resulting in lamellar nanofibrillar structures with lateral dimensions of about 20 nm (figure 15(b)). The π-stacking of P3HT backbones results in the formation of H-aggregated NFs, which was verified by the characteristic changes of optical spectra with the suppression of the longest wavelength, purely electronic transition compared to the vibrational transitions in absorption (compare figures 15(c) and 2). Later, Liu *et al* [124] exploited single- and double-walled carbon nanotubes acting as shishs for the growth P3HT kebabs with similar dimensions.

While those examples provided intriguing proof-of-concepts to create oriented P3HT nanostructures that might be useful for directed energy (or charge) transport along the kebabs, this concept was extended by Bu *et al* [125]. The authors used for both the shish and the kebabs different organic conjugated molecules, i.e., PBI based nanocrystallites as shish for the growth of P3HT kebabs with similar dimensions. Since in this example the absorption characteristics of the shishs and kebabs (after assembly) are slightly different, D–A type structures are formed. Those complex superstructures can be exploited e.g. as antenna systems for light-harvesting with the kebab acting as antenna to collect light and to guide the excitation energy into the shish, from where this energy can then be extracted or converted into charge carriers. The demonstration of superstructures based on two conjugated organic molecules provides many opportunities to create tailor-made excited-state energy landscapes [125, 126]. On the one hand, different chromophores allow to harvest light from a broader spectral range. On the other hand, specific tuning of the excited-state energies of the molecules and of the resulting aggregate structures can be a promising route to create efficient energy funnels for excitons towards artificial reaction centres for energy conversion.

4. Current challenges and future perspectives: important next steps in this field

As discussed in the previous sections, there is currently only a limited number of supramolecular systems available, for which the excited-state energy landscape is known on the level of single nanostructures, and which are suitable to investigate and address long-range energy transport. We believe, however, that this research field holds promise to further shed light on fundamental processes not only in view of efficient light harvesting, but also towards realising truly exciting applications in nanophotonics and optoelectronics once the following challenges related to theoretical aspects, manipulation and characterisation, as well as preparation of novel structures have been addressed:

(a) The theoretical description of both the excited-state energy landscapes and energy transport dynamics has to be further developed. Such modelling is extremely challenging because supramolecular organic nanostructures comprise several 1000s of molecules, the organic molecules exhibit a pronounced vibrational coupling that has to be included, and real nanostructures possess unavoidable intrinsic structural and electronic disorder. In particular, since disorder is both static and dynamic, fluctuations in the electronic Coulomb coupling as well as in the transition energies of each building block have to be considered for a thorough modelling. Further aspects are the refinement and extension of calculations for D–A- and D–A–D-type molecules, in which CT interactions become relevant upon close stacking resulting often in

[11] 'Shish–kebab'-(micro)structure refers originally to a polymer crystallization morphology obtained from solution [122] found in the 60ies. Its shape is reminiscent of a traditional Turkish dish.

unconventional (non-Kasha) photophysics [48, 78]. Important classes of molecules in this context represent dipolar D–A-type merocyanines and quadrupolar squaraines with their D–A–D-structure. Related to simulating energy transport dynamics, there is often a strong discrepancy between experiment and theory, with predicted transport distances and diffusion constants being smaller than those measured in experiments by up to one order of magnitude [88, 127]. In this direction, the description of exciton transport in HJ-aggregates, in which both Coulomb and CT interactions between molecules are relevant, will be a highly interesting avenue [30]. Further advances in modelling are clearly needed to support and to establish guidelines for supramolecular nanostructures with tailored and optimised functionality.

(b) Another underestimated aspect is the preparation, manipulation and characterisation of individual supramolecular nanostructures on the nanoscale. For instance, transfer of nanoobjects to substrates, which is essential to study single objects, should not introduce additional disorder and should not compromise structural integrity. We therefore have to further develop advanced nanoscale preparation, manipulation and characterisation tools for individual supramolecular nanostructures. E.g. FluidFM technology, i.e., AFM in combination with nanofluidics [128], can be beneficially used to prepare and deposit single nanostructures in well-defined arrangements. Moreover, the growth of supramolecular nanostructures along field lines of static electric fields [129] provides intriguing opportunities to create rewritable supramolecular circuits. Finally, optical spectroscopy techniques with ideally single-object sensitivity to avoid averaging over disorder, high time resolution of some femtoseconds and high spatial resolution are required [130–134].

(c) Supramolecular nanostructures with specific properties must be developed. One example would be supramolecular nanostructures that are capable of efficiently transporting both excitation energy as well as charge carriers, which can open new avenues for light-energy conversion. Moreover, supramolecular block copolymers are an emerging class of nanostructures [40, 53], in which each block is assembled from a specific building block (i.e., organic molecule). The molecular interfaces within such supramolecular block copolymers can provide new functionalities, such as charge separation of a neutral exciton or a diode-like behaviour for excitons (and charge carriers) to guide energy only along a specific direction across the interface. An interesting and flexible approach in this direction was reported from the group of Häner, who created alternating H-type stacks of perylene and pyrene chromophores with tuneable composition, using DNA as supramolecular scaffold for their construction [135].

Ultimately, there are ample future perspectives and applications for tailored supramolecular nanostructures. Truly nanophotonic (or excitonic) circuits can be envisioned [136] that exploit (long-range) transport of energy instead of charges. Such circuits can be achieved via a bottom-up approach by applying specific self-assembly protocols. Those circuits can be rewritten due to the reversible nature of non-covalent secondary interactions, instead of employing the currently used top-down approaches resulting in static, hard-wired circuits. Supramolecular nanostructures feature a defined packing of molecules and hence excitation energy can strongly delocalise across many adjacent molecules, i.e., a genuine quantum effect—quantum coherence—is at work, which can be exploited for function. A straightforward function is certainly (partially) coherent energy transport, see section 3.2. However, since an organic molecule (in the two-level approximation, figure 1) can be considered as a qubit (quantum bit), supramolecular systems with their large number of molecules/qubits and their facile scalability might be useful in the field of quantum information science and technology as well [137–140]. Finally, there is also potential of supramolecular systems for neuromorphic computing applications [141, 142] using organic materials. Neuromorphic computing aims to emulate the function of the human brain, which operates highly parallel using a dense network of interconnected neurons. Learning and memory tasks are achieved by changing the connectivity between neurons, the so-called synaptic weights. Here, the dynamic and reversible self-assembly of supramolecular nanostructures can provide opportunities to create the required dynamic wiring between 'artificial' neurons.

To conclude, this review has outlined the exposed position and unique features of functional supramolecular nanostructures. In particular, the defined arrangement of the chromophores as well as the electronic Coulomb interactions between building blocks in such nanostructures provide opportunities to tailor excited-state energy landscapes and thus to add novel properties and functionalities beyond those of the individual chromophores. This often results in unexpected findings and renders this emerging research field an exciting playground for truly novel nanophotonic and optoelectronic applications.

Acknowledgments

We acknowledge financial support from the Bavarian State Ministry of Science and the Arts through the Collaborative Research Network 'Solar Technologies go Hybrid' and the German Research Foundation (DFG)

through the research training group GRK1640. The Elite Network of Bavaria (ENB) through the study programmes 'Biological Physics' and 'Macromolecular Science' is gratefully acknowledged. We thank Sebastian Stäter, Bernd Wittmann and Felix Wenzel for their help with some of the figures and fruitful discussion. We are also grateful to our collaborators who contributed to this line of research in previous years.

Data availability statement

No new data were created or analysed in this study.

ORCID iDs

Klaus Kreger https://orcid.org/0000-0003-3021-1311
Hans-Werner Schmidt https://orcid.org/0000-0002-1761-1153
Richard Hildner https://orcid.org/0000-0002-7282-3730

References

[1] Scholes G D, Fleming G R, Olaya-Castro A and van Grondelle R 2011 Lessons from nature about solar light harvesting *Nat. Chem.* **3** 763–74
[2] Hu X, Ritz T, Damjanović A, Autenrieth F and Schulten K 2002 Photosynthetic apparatus of purple bacteria *Q. Rev. Biophys.* **35** 1–62
[3] Cogdell R J, Gall A and Köhler J 2006 The architecture and function of the light-harvesting apparatus of purple bacteria: from single molecules to *in vivo* membranes *Q. Rev. Biophys.* **39** 227–324
[4] Strümpfer J, Şener M and Schulten K 2012 How quantum coherence assists photosynthetic light-harvesting *J. Phys. Chem. Lett.* **3** 536–42
[5] Scholes G D *et al* 2017 Using coherence to enhance function in chemical and biophysical systems *Nature* **543** 647–56
[6] Ball P 2011 Physics of life: the dawn of quantum biology *Nature* **474** 272–4
[7] Scholes G D 2010 Quantum-coherent electronic energy transfer: did nature think of it first? *J. Phys. Chem. Lett.* **1** 2–8
[8] Romero E, Novoderezhkin V I and van Grondelle R 2017 Quantum design of photosynthesis for bio-inspired solar-energy conversion *Nature* **543** 355–65
[9] Brédas J-L, Sargent E H and Scholes G D 2016 Photovoltaic concepts inspired by coherence effects in photosynthetic systems *Nat. Mater.* **16** 35–44
[10] Scholes G D, Mirkovic T, Turner D B, Fassioli F and Buchleitner A 2012 Solar light harvesting by energy transfer: from ecology to coherence *Energy Environ. Sci.* **5** 9374
[11] Scholes G D 2003 Long-range resonance energy transfer in molecular systems *Annu. Rev. Phys. Chem.* **54** 57–87
[12] Scholes G D and Rumbles G 2006 Excitons in nanoscale systems *Nat. Mater.* **5** 683–96
[13] Henson Z B, Müllen K and Bazan G C 2012 Design strategies for organic semiconductors beyond the molecular formula *Nat. Chem.* **4** 699–704
[14] Gierschner J 2012 Directional exciton transport in supramolecular nanostructured assemblies *Phys. Chem. Chem. Phys.* **14** 13146–53
[15] Caram J R, Doria S, Eisele D M, Freyria F S, Sinclair T S, Rebentrost P, Lloyd S and Bawendi M G 2016 Room-temperature micron-scale exciton migration in a stabilized emissive molecular aggregate *Nano Lett.* **16** 6808–15
[16] Schmidt H W and Würthner F 2020 A periodic system of supramolecular elements *Angew. Chem., Int. Ed.* **59** 8766–75
[17] Brixner T, Hildner R, Köhler J, Lambert C and Würthner F 2017 Exciton transport in molecular aggregates—from natural antennas to synthetic chromophore systems *Adv. Energy Mater.* **7** 1700236
[18] Spano F C 2005 Modeling disorder in polymer aggregates: the optical spectroscopy of regioregular poly(3-hexylthiophene) thin films *J. Chem. Phys.* **122** 234701
[19] Spano F C 2010 The spectral signatures of Frenkel polarons in H- and J-aggregates *Acc. Chem. Res.* **43** 429–39
[20] Kasha M 1963 Energy transfer mechanisms and the molecular exciton model for molecular aggregates *Radiat. Res.* **20** 55
[21] Kasha M, Rawls H R and Ashraf El-Bayoumi M 1965 The exciton model in molecular spectroscopy *Pure Appl. Chem.* **11** 371–92
[22] Davydov A S 1971 *Theory of Molecular Excitons* (Berlin: Springer)
[23] Schwoerer M and Wolf H C 2008 *Organic Molecular Solids* (New York: Wiley)
[24] Köhler A and Bässler H 2015 *Electronic Processes in Organic Semiconductors: An Introduction* (New York: Wiley)
[25] Philpott M R 1971 Theory of the coupling of electronic and vibrational excitations in molecular crystals and helical polymers *J. Chem. Phys.* **55** 2039–54
[26] Hestand N J and Spano F C 2017 Molecular aggregate photophysics beyond the Kasha model: novel design principles for organic materials *Acc. Chem. Res.* **50** 341–50
[27] Hestand N J and Spano F C 2018 Expanded theory of H- and J-molecular aggregates: the effects of vibronic coupling and intermolecular charge transfer *Chem. Rev.* **118** 7069–163
[28] Hestand N J, Kazantsev R V, Weingarten A S, Palmer L C, Stupp S I and Spano F C 2016 Extended-charge-transfer excitons in crystalline supramolecular photocatalytic scaffolds *J. Am. Chem. Soc.* **138** 11762–74
[29] Austin A, Hestand N J, McKendry I G, Zhong C, Zhu X, Zdilla M J, Spano F C and Szarko J M 2017 Enhanced Davydov splitting in crystals of a perylene diimide derivative *J. Phys. Chem. Lett.* **8** 1118–23
[30] Oleson A *et al* 2019 Perylene diimide-based Hj- and hJ-aggregates: the prospect of exciton band shape engineering in organic materials *J. Phys. Chem.* C **123** 20567–78
[31] Jelly E E 1936 Spectral absorption and fluorescence of dyes in the molecular state *Nature* **138** 1009–10
[32] Scheibe G 1936 Über die Veränderlichkeit des Absorptionsspektrums einiger Sensibilisierungsfarbstoffe und deren Ursache Chemie *Angew. Chem.* **49** 563

[33] Scheibe G, Kandler L and Ecker H 1937 Polymerisation und polymere Adsorption als Ursache neuartiger Absorptionsbanden von organischen Farbstoffen *Naturwissenschaften* **25** 75
[34] Sasaki N *et al* 2020 Supramolecular double-stranded Archimedean spirals and concentric toroids *Nat. Commun.* **11** 3578
[35] Brunsveld L, Folmer B J B, Meijer E W and Sijbesma R P 2001 Supramolecular polymers *Chem. Rev.* **101** 4071–98
[36] de Greef T F A, Smulders M M J, Wolffs M, Schenning A P H J, Sijbesma R P and Meijer E W 2009 Supramolecular polymerization *Chem. Rev.* **109** 5687–754
[37] Aida T, Meijer E W and Stupp S I 2012 Functional supramolecular polymers *Science* **335** 813–7
[38] Clemons T D and Stupp S I 2020 Design of materials with supramolecular polymers *Prog. Polym. Sci.* **111** 101310
[39] Aida T and Meijer E W 2020 Supramolecular polymers—we've come full circle *Isr. J. Chem.* **60** 33–47
[40] Wehner M and Würthner F 2020 Supramolecular polymerization through kinetic pathway control and living chain growth *Nat. Rev. Chem.* **4** 38–53
[41] Hashim P K, Bergueiro J, Meijer E W and Aida T 2020 Supramolecular polymerization: a conceptual expansion for innovative materials *Prog. Polym. Sci.* **105** 101250
[42] Würthner F, Kaiser T E and Saha-Möller C R 2011 J-aggregates: from serendipitous discovery to supramolecular engineering of functional dye materials *Angew. Chem., Int. Ed.* **50** 3376–410
[43] Eisele D M *et al* 2014 Robust excitons inhabit soft supramolecular nanotubes *Proc. Natl Acad. Sci.* **111** E3367–75
[44] Deshmukh A P, Bailey A D, Forte L S, Shen X, Geue N, Sletten E M and Caram J R 2020 Thermodynamic control over molecular aggregate assembly enables tunable excitonic properties across the visible and near-infrared *J. Phys. Chem. Lett.* **11** 8026–33
[45] Hu X, Lindner J O and Würthner F 2020 Stepwise folding and self-assembly of a merocyanine folda-pentamer *J. Am. Chem. Soc.* **142** 3321–5
[46] Zhang Y, Kim B, Yao S, Bondar M V and Belfield K D 2013 Controlled aggregation and enhanced two-photon absorption of a water-soluble squaraine dye with a poly(acrylic acid) template *Langmuir* **29** 11005–12
[47] Liess A, Lv A, Arjona-Esteban A, Bialas D, Krause A-M, Stepanenko V, Stolte M and Würthner F 2017 Exciton coupling of merocyanine dyes from H- to J-type in the solid state by crystal engineering *Nano Lett.* **17** 1719–26
[48] Sanyal S, Painelli A, Pati S K, Terenziani F and Sissa C 2016 Aggregates of quadrupolar dyes for two-photon absorption: the role of intermolecular interactions *Phys. Chem. Chem. Phys.* **18** 28198–208
[49] Kaczmarek-Kdziera A, Żuchowski P S and Kdziera D 2020 Nature of intermolecular interaction in squaraine dimers *Sci. Rep.* **10** 19670
[50] Hestand N J, Zheng C, Penmetcha A R, Cona B, Cody J A, Spano F C and Collison C J 2015 Confirmation of the origins of panchromatic spectra in squaraine thin films targeted for organic photovoltaic devices *J. Phys. Chem.* C **119** 18964–74
[51] Basak S, Nandi N, Baral A and Banerjee A 2015 Tailor-made design of J- or H-aggregated naphthalenediimide-based gels and remarkable fluorescence turn on/off behaviour depending on solvents *Chem. Commun.* **51** 780–3
[52] Kar H, Gehrig D W, Allampally N K, Fernández G, Laquai F and Ghosh S 2016 Cooperative supramolecular polymerization of an amine-substituted naphthalene-diimide and its impact on excited state photophysical properties *Chem. Sci.* **7** 1115–20
[53] Wagner W, Wehner M, Stepanenko V, Ogi S and Würthner F 2017 Living supramolecular polymerization of a perylene bisimide dye into fluorescent J-aggregates *Angew. Chem., Int. Ed.* **56** 16008–12
[54] Greciano E E, Calbo J, Ortí E and Sánchez L 2020 N-annulated perylene bisimides to bias the differentiation of metastable supramolecular assemblies into J- and H-aggregates *Angew. Chem., Int. Ed.* **59** 17517–24
[55] Haedler A T, Kreger K, Issac A, Wittmann B, Kivala M, Hammer N, Köhler J, Schmidt H-W and Hildner R 2015 Long-range energy transport in single supramolecular nanofibres at room temperature *Nature* **523** 196–9
[56] Haedler A T, Meskers S C J, Zha R H, Kivala M, Schmidt H-W and Meijer E W 2016 Pathway complexity in the enantioselective self-assembly of functional carbonyl-bridged triarylamine trisamides *J. Am. Chem. Soc.* **138** 10539–45
[57] Ogi S, Fukui T, Jue M L, Takeuchi M and Sugiyasu K 2014 Kinetic control over pathway complexity in supramolecular polymerization through modulating the energy landscape by rational molecular design *Angew. Chem., Int. Ed.* **53** 14363–7
[58] van der Weegen R, Teunissen A J P and Meijer E W 2017 Directing the self-assembly behaviour of porphyrin-based supramolecular systems *Chem. Eur. J.* **23** 3773–83
[59] Zhang W, Jin W, Fukushima T, Saeki A, Seki S and Aida T 2011 Supramolecular linear heterojunction composed of graphite-like semiconducting nanotubular segments *Science* **334** 340–3
[60] Zhang W, Jin W, Fukushima T, Mori T and Aida T 2015 Helix sense-selective supramolecular polymerization seeded by a one-handed helical polymeric assembly *J. Am. Chem. Soc.* **137** 13792–5
[61] Martinez C R and Iverson B L 2012 Rethinking the term 'pi-stacking' *Chem. Sci.* **3** 2191
[62] Li Q and Li Z 2017 The strong light-emission materials in the aggregated state: what happens from a single molecule to the collective group *Adv. Sci.* **4** 1600484
[63] Jonkheijm P, van der Schoot P, Schenning A P H J and Meijer E W 2006 Probing the solvent-assisted nucleation pathway in chemical self-assembly *Science* **313** 80–3
[64] Korevaar P A, George S J, Markvoort A J, Smulders M M J, Hilbers P A J, Schenning A P H J, de Greef T F A and Meijer E W 2012 Pathway complexity in supramolecular polymerization *Nature* **481** 492–6
[65] Dumele O, Chen J, Passarelli J V and Stupp S I 2020 Supramolecular energy materials *Adv. Mater.* **32** e1907247
[66] Herbst S, Soberats B, Leowanawat P, Stolte M, Lehmann M and Würthner F 2018 Self-assembly of multi-stranded perylene dye J-aggregates in columnar liquid-crystalline phases *Nat. Commun.* **9** 2646
[67] Haedler A T, Beyer S R, Hammer N, Hildner R, Kivala M, Köhler J and Schmidt H-W 2014 Synthesis and photophysical properties of multichromophoric carbonyl-bridged triarylamines *Chem. Eur. J.* **20** 11708–18
[68] Wittmann B *et al* 2020 Enhancing long-range energy transport in supramolecular architectures by tailoring coherence properties *J. Am. Chem. Soc.* **142** 8323–30
[69] Liess A, Arjona-Esteban A, Kudzus A, Albert J, Krause A M, Lv A, Stolte M, Meerholz K and Würthner F 2019 Ultranarrow bandwidth organic photodiodes by exchange narrowing in merocyanine H- and J-aggregate excitonic systems *Adv. Funct. Mater.* **29** 1805058
[70] Matern J, Dorca Y, Sánchez L and Fernández G 2019 Revising complex supramolecular polymerization under kinetic and thermodynamic control *Angew. Chem., Int. Ed.* **58** 16730–40
[71] Korevaar P A, de Greef T F A and Meijer E W 2014 Pathway complexity in π-conjugated materials *Chem. Mater.* **26** 576–86
[72] Chen Z, Liu Y, Wagner W, Stepanenko V, Ren X, Ogi S and Würthner F 2017 Near-IR absorbing J-aggregate of an amphiphilic BF_2-azadipyrromethene dye by kinetic cooperative self-assembly *Angew. Chem., Int. Ed.* **56** 5729–33

[73] Fukui T, Kawai S, Fujinuma S, Matsushita Y, Yasuda T, Sakurai T, Seki S, Takeuchi M and Sugiyasu K 2017 Control over differentiation of a metastable supramolecular assembly in one and two dimensions *Nat. Chem.* **9** 493–9

[74] Ogi S, Sugiyasu K, Manna S, Samitsu S and Takeuchi M 2014 Living supramolecular polymerization realized through a biomimetic approach *Nat. Chem.* **6** 188–95

[75] Ogi S, Grzeszkiewicz C and Würthner F 2018 Pathway complexity in the self-assembly of a zinc chlorin model system of natural bacteriochlorophyll J-aggregates *Chem. Sci.* **9** 2768–73

[76] Valera J S, Sánchez-Naya R, Ramírez F J, Zafra J L, Gómez R, Casado J and Sánchez L 2017 Solvent-directed helical stereomutation discloses pathway complexity on N-heterotriangulene-based organogelators *Chem. Eur. J.* **23** 11141–6

[77] Valera J S, Gómez R and Sánchez L 2018 Tunable energy landscapes to control pathway complexity in self-assembled N-heterotriangulenes: living and seeded supramolecular polymerization *Small* **14** 1702437

[78] Zheng C, Zhong C, Collison C J and Spano F C 2019 Non-Kasha behavior in quadrupolar dye aggregates: the red-shifted H-aggregate *J. Phys. Chem.* C **123** 3203–15

[79] Wehner M, Röhr M I S, Bühler M, Stepanenko V, Wagner W and Würthner F 2019 Supramolecular polymorphism in one-dimensional self-assembly by kinetic pathway control *J. Am. Chem. Soc.* **141** 6092–107

[80] Wagner W, Wehner M, Stepanenko V and Würthner F 2019 Supramolecular block copolymers by seeded living polymerization of perylene bisimides *J. Am. Chem. Soc.* **141** 12044–54

[81] Martin-Martinez F J, Jin K, López Barreiro D and Buehler M J 2018 The rise of hierarchical nanostructured materials from renewable sources: learning from nature *ACS Nano* **12** 7425–33

[82] Wang A, Huang J and Yan Y 2014 Hierarchical molecular self-assemblies: construction and advantages *Soft Matter* **10** 3362–73

[83] Moulin E, Armao J J and Giuseppone N 2019 Triarylamine-based supramolecular polymers: structures, dynamics, and functions *Acc. Chem. Res.* **52** 975–83

[84] Lu Y, Lin J, Wang L, Zhang L and Cai C 2020 Self-assembly of copolymer micelles: higher-level assembly for constructing hierarchical structure *Chem. Rev.* **120** 4111–40

[85] Marty R *et al* 2013 Hierarchically structured microfibers of 'single stack' perylene bisimide and quaterthiophene nanowires *ACS Nano* **7** 8498–508

[86] Vlaming S M, Augulis R, Stuart M C A, Knoester J and van Loosdrecht P H M 2009 Exciton spectra and the microscopic structure of self-assembled porphyrin nanotubes *J. Phys. Chem.* B **113** 2273–83

[87] Kim T, Ham S, Lee S H, Hong Y and Kim D 2018 Enhancement of exciton transport in porphyrin aggregate nanostructures by controlling the hierarchical self-assembly *Nanoscale* **10** 16438–46

[88] Wan Y, Stradomska A, Knoester J and Huang L 2017 Direct imaging of exciton transport in tubular porphyrin aggregates by ultrafast microscopy *J. Am. Chem. Soc.* **139** 7287–93

[89] Eisele D M *et al* 2012 Utilizing redox-chemistry to elucidate the nature of exciton transitions in supramolecular dye nanotubes *Nat. Chem.* **4** 655–62

[90] Kriete B, Bondarenko A S, Jumde V R, Franken L E, Minnaard A J, Jansen T L C, Knoester J and Pshenichnikov M S 2017 Steering self-assembly of amphiphilic molecular nanostructures via halogen exchange *J. Phys. Chem. Lett.* **8** 2895–901

[91] Kriete B, Bondarenko A S, Alessandri R, Patmanidis I, Krasnikov V V, Jansen T L C, Marrink S J, Knoester J and Pshenichnikov M S 2020 Molecular versus excitonic disorder in individual artificial light-harvesting systems *J. Am. Chem. Soc.* **142** 18073–85

[92] Bondarenko A S, Jansen T L C and Knoester J 2020 Exciton localization in tubular molecular aggregates: size effects and optical response *J. Chem. Phys.* **152** 194302

[93] Kriete B, Lüttig J, Kunsel T, Malý P, Jansen T L C, Knoester J, Brixner T and Pshenichnikov M S 2019 Interplay between structural hierarchy and exciton diffusion in artificial light harvesting *Nat. Commun.* **10** 4615

[94] Clark K A, Krueger E L and Vanden Bout D A 2014 Direct measurement of energy migration in supramolecular carbocyanine dye nanotubes *J. Phys. Chem. Lett.* **5** 2274–82

[95] Knapp E W 1984 Lineshapes of molecular aggregates, exchange narrowing and intersite correlation *Chem. Phys.* **85** 73–82

[96] Spano F C, Clark J, Silva C and Friend R H 2009 Determining exciton coherence from the photoluminescence spectral line shape in poly(3-hexylthiophene) thin films *J. Chem. Phys.* **130** 074904

[97] Moix J M, Khasin M and Cao J 2013 Coherent quantum transport in disordered systems: I. The influence of dephasing on the transport properties and absorption spectra on one-dimensional systems *New J. Phys.* **15** 085010

[98] Mohseni M, Aspuru-Guzik A, Rebentrost P, Shabani A, Lloyd S, Huelga S F and Plenio M B 2014 Environment-assisted quantum transport *Quantum Effects in Biology* ed M Mohseni (Cambridge: Cambridge University Press) pp 159–76

[99] Novo L, Mohseni M and Omar Y 2016 Disorder-assisted quantum transport in suboptimal decoherence regimes *Sci. Rep.* **6** 18142

[100] Lin H, Camacho R, Tian Y, Kaiser T E, Wu¨rthner F and Scheblykin I G 2010 Collective fluorescence blinking in linear J-aggregates assisted by long-distance exciton migration *Nano Lett.* **10** 620–6

[101] Rehhagen C, Stolte M, Herbst S, Hecht M, Lochbrunner S, Würthner F and Fennel F 2020 Exciton migration in multistranded perylene bisimide J-aggregates *J. Phys. Chem. Lett.* **11** 6612–7

[102] Akselrod G M, Tischler Y R, Young E R, Nocera D G and Bulovic V 2010 Exciton–exciton annihilation in organic polariton microcavities *Phys. Rev.* B **82** 113106

[103] Eisele D M, Knoester J, Kirstein S, Rabe J P and Vanden Bout D A 2009 Uniform exciton fluorescence from individual molecular nanotubes immobilized on solid substrates *Nat. Nanotechnol.* **4** 658–63

[104] Winiger C B, Li S, Kumar G R, Langenegger S M and Häner R 2014 Long-distance electronic energy transfer in light-harvesting supramolecular polymers *Angew. Chem., Int. Ed.* **53** 13609–13

[105] Jevric J, Langenegger S M and Häner R 2020 Light-harvesting supramolecular polymers: energy transfer to various polyaromatic acceptors *Eur. J. Org. Chem.* **2020** 4677–80

[106] Merdasa A, Jiménez Á J, Camacho R, Meyer M, Würthner F and Scheblykin I G 2014 Single Lévy states-disorder induced energy funnels in molecular aggregates *Nano Lett.* **14** 6774–81

[107] Solomon L A, Sykes M E, Wu Y A, Schaller R D, Wiederrecht G P and Fry H C 2017 Tailorable exciton transport in doped peptide-amphiphile assemblies *ACS Nano* **11** 9112–8

[108] Armao J J, Rabu P, Moulin E and Giuseppone N 2016 Long-range energy transport via plasmonic propagation in a supramolecular organic waveguide *Nano Lett.* **16** 2800–5

[109] Scheibe G, Schöntag A and Katheder F 1939 Fluoreszenz und Energiefortleitung bei reversibel polymerisierten Farbstoffen *Naturwissenschaften* **27** 499–501

[110] Avakian P and Merrifield R E 1964 Experimental determination of the diffusion length of triplet excitons in anthracene crystals *Phys. Rev. Lett.* **13** 541–3

[111] Wan Y, Guo Z, Zhu T, Yan S, Johnson J and Huang L 2015 Cooperative singlet and triplet exciton transport in tetracene crystals visualized by ultrafast microscopy *Nat. Chem.* **7** 785–92
[112] Akselrod G M, Deotare P B, Thompson N J, Lee J, Tisdale W A, Baldo M A, Menon V M and Bulović V 2014 Visualization of exciton transport in ordered and disordered molecular solids *Nat. Commun.* **5** 3646
[113] Menke S M and Holmes R J 2014 Exciton diffusion in organic photovoltaic cells *Energy Environ. Sci.* **7** 499–512
[114] Lin J D A *et al* 2014 Systematic study of exciton diffusion length in organic semiconductors by six experimental methods *Mater. Horiz.* **1** 280–5
[115] Mikhnenko O V, Blom P W M and Nguyen T-Q 2015 Exciton diffusion in organic semiconductors *Energy Environ. Sci.* **8** 1867–88
[116] Topczak A K, Roller T, Engels B, Brütting W and Pflaum J 2014 Nonthermally activated exciton transport in crystalline organic semiconductor thin films *Phys. Rev.* B **89** 201203
[117] Wittmann B, Wiesneth S, Motamen S, Simon L, Serein-Spirau F, Reiter G and Hildner R 2020 Energy transport and light propagation mechanisms in organic single crystals *J. Chem. Phys.* **153** 144202
[118] Simpson O 1957 Electronic properties of aromatic hydrocarbons. III. Diffusion of excitons *Proc. R. Soc.* A **238** 402–11
[119] Vlaming S M, Malyshev V A, Eisfeld A and Knoester J 2013 Subdiffusive exciton motion in systems with heavy-tailed disorder *J. Chem. Phys.* **138** 214316
[120] Wiesenhofer H, Beljonne D, Scholes G D, Hennebicq E, Brédas J-L and Zojer E 2005 Limitations of the Förster description of singlet exciton migration: the illustrative example of energy transfer to ketonic defects in ladder-type poly(para-phenylenes) *Adv. Funct. Mater.* **15** 155–60
[121] Zhang L, Zhong X, Pavlica E, Li S, Klekachev A, Bratina G, Ebbesen T W, Orgiu E and Samorì P 2016 A nanomesh scaffold for supramolecular nanowire optoelectronic devices *Nat. Nanotechnol.* **11** 900–6
[122] Keller A and Machin M J 1967 Oriented crystallization in polymers *J. Macromol. Sci.* B **1** 41–91
[123] Brinkmann M, Chandezon F, Pansu R B and Julien-Rabant C 2009 Epitaxial growth of highly oriented fibers of semiconducting polymers with a shish–kebab-like superstructure *Adv. Funct. Mater.* **19** 2759–66
[124] Liu J, Zou J and Zhai L 2009 Bottom-up assembly of poly(3-hexylthiophene) on carbon nanotubes: 2D building blocks for nanoscale circuits *Macromol. Rapid Commun.* **30** 1387–91
[125] Bu L, Pentzer E, Bokel F A, Emrick T and Hayward R C 2012 Growth of polythiophene/perylene tetracarboxydiimide donor/acceptor shish–kebab nanostructures by coupled crystal modification *ACS Nano* **6** 10924–9
[126] Rieth S, Li Z, Hinkle C E, Guzman C X, Lee J J, Nehme S I and Braunschweig A B 2013 Superstructures of diketopyrrolopyrrole donors and perylenediimide acceptors formed by hydrogen-bonding and $\pi\cdots\pi$ stacking *J. Phys. Chem.* C **117** 11347–56
[127] Saikin S K, Shakirov M A, Kreisbeck C, Peskin U, Proshin Y N and Aspuru-Guzik A 2017 On the long-range exciton transport in molecular systems: the application to H-aggregated heterotriangulene chains *J. Phys. Chem.* C **121** 24994–5002
[128] Helfricht N, Mark A, Behr M, Bernet A, Schmidt H-W and Papastavrou G 2017 Writing with fluid: structuring hydrogels with micrometer precision by AFM in combination with nanofluidics *Small* **13** 1700962
[129] Moulin E, Cid J-J and Giuseppone N 2013 Advances in supramolecular electronics—from randomly self-assembled nanostructures to addressable self-organized interconnects *Adv. Mater.* **25** 477–87
[130] Zhu T, Wan Y and Huang L 2017 Direct imaging of Frenkel exciton transport by ultrafast microscopy *Acc. Chem. Res.* **50** 1725–33
[131] Pandya R *et al* 2020 Femtosecond transient absorption microscopy of singlet exciton motion in side-chain engineered perylene-diimide thin films *J. Phys. Chem.* A **124** 2721–30
[132] Schnedermann C, Sung J, Pandya R, Verma S D, Chen R Y S, Gauriot N, Bretscher H M, Kukura P and Rao A 2019 Ultrafast tracking of exciton and charge carrier transport in optoelectronic materials on the nanometer scale *J. Phys. Chem. Lett.* **10** 6727–33
[133] Penwell S B, Ginsberg L D S, Noriega R and Ginsberg N S 2017 Resolving ultrafast exciton migration in organic solids at the nanoscale *Nat. Mater.* **16** 1136–41
[134] Ginsberg N S and Tisdale W A 2020 Spatially resolved photogenerated exciton and charge transport in emerging semiconductors *Annu. Rev. Phys. Chem.* **71** 1–30
[135] Winiger C B, Langenegger S M, Calzaferri G and Häner R 2015 Formation of two homo-chromophoric H-aggregates in DNA-assembled alternating dye stacks *Angew. Chem., Int. Ed.* **54** 3643–7
[136] Park H *et al* 2016 Enhanced energy transport in genetically engineered excitonic networks *Nat. Mater.* **15** 211–6
[137] Reina J H, Susa C E and Hildner R 2018 Conditional quantum dynamics and nonlocal states in dimeric and trimeric arrays of organic molecules *Phys. Rev.* A **97** 063422
[138] Arute F *et al* 2019 Quantum supremacy using a programmable superconducting processor *Nature* **574** 505–10
[139] Preskill J 2018 Quantum computing in the NISQ era and beyond *Quantum* **2** 79
[140] Wasielewski M R *et al* 2020 Exploiting chemistry and molecular systems for quantum information science *Nat. Rev. Chem.* **4** 490–504
[141] van de Burgt Y, Melianas A, Keene S T, Malliaras G and Salleo A 2018 Organic electronics for neuromorphic computing *Nat. Electron.* **1** 386–97
[142] Valov I and Kozicki M 2017 Non-volatile memories: organic memristors come of age *Nat. Mater.* **16** 1170–2